

# Integrated Light 2MASS IR Photometry of Galactic Globular Clusters

Judith G. Cohen<sup>2</sup>, Scott Hsieh<sup>2</sup>, Stanimir Metchev<sup>3</sup>, S. G. Djorgovski<sup>2</sup> & M. Malkan<sup>3</sup>

## ABSTRACT

We have mosaiced 2MASS images to derive surface brightness profiles in  $J$ ,  $H$  and  $K_s$  for 104 Galactic globular clusters. We fit these with King profiles, and show that the core radii are identical to within the errors for each of these IR colors, and are identical to the core radii at  $V$  in essentially all cases. We derive integrated light colors  $V - J$ ,  $V - H$ ,  $V - K_s$ ,  $J - H$  and  $J - K_s$  for these globular clusters. Each color shows a reasonably tight relation between the dereddened colors and metallicity. Fits to these are given for each color. The IR–IR colors have very small errors due largely to the all-sky photometric calibration of the 2MASS survey, while the  $V$ –IR colors have substantially larger uncertainties. We find fairly good agreement with measurements of integrated light colors for a smaller sample of Galactic globular clusters by Aaronson, Malkan & Kleinmann from 1977. Our results provide a calibration for the integrated light of distant single burst old stellar populations from very low to Solar metallicities. A comparison of our dereddened measured colors with predictions from several models of the integrated light of single burst old populations shows good agreement in the low metallicity domain for  $V - K_s$  colors, but an offset at a fixed  $[\text{Fe}/\text{H}]$  of  $\sim 0.1$  mag in  $J - K_s$ , which we ascribe to photometric system transformation issues. Some of the models fail to reproduce the behavior of the integrated light colors of the Galactic globular clusters near Solar metallicity.

*Subject headings:* globular clusters: general — galaxies: star clusters

## 1. Introduction

Galactic globular clusters (GCs) are of great interest as nearby representatives of simple stellar systems all of whose stars share the same age and initial chemical composition<sup>1</sup>. They are close enough that individual stars can be studied in detail with spectroscopy and photometry, while far enough away that, with some difficulty, their integrated light can be measured as well. Their

---

<sup>2</sup>Palomar Observatory, Mail Stop 105-24, California Institute of Technology, Pasadena, Ca., 91125, jlc(george)@astro.caltech.edu, scottshsieh@gmail.com

<sup>3</sup>Department of Physics and Astronomy, University of California, Los Angeles, Ca. 90095, metchev(malkan)@astro.ucla.edu

<sup>1</sup>We ignore the anomalous GC  $\omega$  Cen here.

ages and initial mass functions can be determined through analysis of deep high spatial resolution imaging, primarily from HST; mass segregation can be studied for these objects as well. Integrated light measurements of Galactic GCs are of key importance as they provide calibration data for the study of more distant early type galaxies with predominantly old populations as well as the GCs of distant galaxies for which only the integrated light can be observed.

The Two Micron All Sky Survey (2MASS) affords us a wonderful opportunity to study the surface brightness profiles of nearby GCs in the infrared. As described in detail by Skrutskie *et al.* (2006), two 1.3m diameter telescopes were used, one in the northern and one in the southern hemisphere. The whole sky was observed in three colors,  $J$ ,  $H$ , and  $K_s$  (a variant of the  $K$  filter described in detail therein). The advantages for our purposes of the 2MASS data over any previously existing are many. The photometry is all-sky with careful attention to calibration issues, ensuring uniformity over all the frames. The database is digital, and hence background subtraction and sophisticated image analyses are feasible. There are, of course, disadvantages as well. The effective exposure time for each point in the sky in this survey was short, only 7.8 sec in each of the three colors, so these images reach a relatively shallow limiting magnitude. Furthermore the spatial resolution is limited by the adopted detector pixel size of 2.0" on a side.

## 2. The Surface Brightness Profiles from 2MASS

We describe here the process we have used to define and fit the surface brightness profile of Galactic GCs in  $J$ ,  $H$  and  $K_s$  from the 2MASS data. The integrated light in the IR is sensitive to rare bright RGB tip giants and AGB stars. Hence centroiding in the IR is more subject to stochastic effects dependent on cluster richness than it is at optical wavelengths, where the numerous stars near the main sequence turnoff make a substantial contribution to the integrated light. We therefore begin by adopting the GC cluster centers determined from the on-line database for the Galactic GC system maintained by W. Harris (Harris 1996)<sup>2</sup>, as updated in 2003 (henceforth H96). These were derived from optical images of the GCs. The tidal radii of GCs are determined by the gravitational field of the Galaxy. Furthermore, there is no hope of accurately measuring the surface brightness profile in the outermost parts of the Galactic GCs from the short and relatively shallow 2MASS exposures as the GCs are often very extended and the surface brightness near the tidal radius ( $r_t$ ) is low. We thus adopt the values of  $r_t$  determined from optical photometry as compiled in the same on-line database; these are primarily from Trager, King & Djorgovski (1995) (henceforth TKD95).

A square region, centered on the GC and with a side length of  $2r_t$ , was used for each cluster. We downloaded the FITS image files from the 2MASS website Batch Image service that cover the required area for each Galactic GC for each of the three filters  $J$ ,  $H$  and  $K_s$ . The most extended GCs (clusters with  $r_t \gtrsim 0.45^\circ$ ) are likely to have some missing data (not a problem), and those

---

<sup>2</sup>at <http://physwww.mcmaster.ca/~Eharris/WEHarris.html>

with  $r_t \gtrsim 0.6^\circ$  ( $\sim 5$  Galactic GCs) could not be analyzed at all due to excessive memory and CPU requirements. Data for one such very extended GC, 47 Tuc, was recovered from the 2MASS Large Galaxy Catalog.

Processed frames from 2MASS have  $1.0'' \times 1.0''$  pixels and are tiled together in a regular fashion, with an overlap region between frames. The individual frames were made into a mosaic for each GC in each of the three IR colors by examining the header in each FITS file to determine if it had neighboring frames adjacent to it, and then removing duplicated points in the overlap regions. Because the tiling was not perfectly gridlike but rather somewhat staggered, a few duplicate points were left behind and a few other points were removed that should have been kept, but this should have a negligible effect. When the frames were irregularly stacked (as was the case in certain clusters), the mosaic procedure failed. This was fixed when it was not too difficult to do so by deleting selected frames from the data set; less than 5 GCs were handled this way.

Frames were adjusted to a constant sky value and calibrated to a universal adopted magnitude zero point for each color; we adopted values typical of those on the 2MASS images, specifically 20.45, 20.90, and 19.93 mag DN<sup>-1</sup> arcsec<sup>-2</sup> for  $J$ ,  $H$  and  $K_s$ , respectively. The calculation relies on the photometric zero point determined for each frame by the 2MASS project which is given in the keyword MAGZP in the header of each image. Extinction within the Earth’s atmosphere is included in these zero points. The value of each pixel is reset to reflect the different depth achieved by each particular frame in the mosaic for each GC in each of the three colors. The sky value for each GC at each of  $J$ ,  $H$  and  $K_s$  was simply taken to be the mean sky value of the individual rescaled frames, as indicated by the keyword SKY in the FITS header of each file. A detailed discussion of the algorithms used by the 2MASS project to determine the values of these parameters for each frame is given in Cutri *et al.* (2003). The background from non-member stars in the region of each GC was evaluated in a region largely beyond the tidal radius, extending from 0.95 to 2.0  $r_t$ .

The calculation of the surface brightness followed that of Fischer *et al.* (1992), based on the method of Djorgovski (1986). The image was divided into several annuli centered on the globular cluster. The 2MASS detector pixels are  $2.0''$  on a side, so the first annulus was a circle with a  $5''$  radius. Subsequent annuli went from  $5''$  to 95% of the tidal radius, with the annuli evenly spaced in logarithmic space. If  $r_t < 5'$ , 8 annuli were used; if less than  $10'$ , 10 annuli were used; if greater than  $10'$ , 15 annuli were used. The effective radius,  $r_{eff}$ , assigned to each annulus is the intensity-weighted mean radius of the annulus (under the assumption of a linear intensity profile over the width of the annulus; Newell & O’Neil 1978),

$$r_{eff} = \frac{2r_2^3 - r_1^3}{3r_2^2 - r_1^2},$$

where  $r_1$  and  $r_2$  are the inner and outer radii of the annulus.

Each annulus was divided into eight  $45^\circ$  sectors, and the mean DN of the pixels within each

sector was found. In the first annulus (actually circle), as well as all annuli with  $r_{eff} < 10''$ , the mean of the 8 sector means was used as the surface brightness within that annulus, since the variations among the sectors for a given  $r_{eff}$  arise primarily from possible stochastic fluctuations and potential errors in the adopted position of the cluster center rather than from photometric errors or from non-member stars. For annuli with  $r_{eff} > 10''$ , the median of these 8 sector means (in practice the average of the fourth and fifth value of the sorted list) was chosen as the final value for that annulus. Use of the median minimizes the surface brightness fluctuations due to a small number of bright stars, but biases the mean surface brightness towards lower values, since it effectively excludes some light from the brightest red giants; however, this surface brightness profile is more representative of the bulk of the stellar population in the cluster.

## 2.1. Globular Cluster Centers

We initially adopt the centers of the GCs from the 2003 on line version of the database of Harris (1996). The majority of the cluster center coordinates in both H96 and in Djorgovski & Meylan (1993) are from Shawl & White (1986), and for most cases they are not expected to be determined better than to a few arcsec. While the centers from H96 generally appeared to be correct, sometimes they seemed not to coincide with the center of a few of the GCs as judged from the 2MASS images. An effort was made to develop a centroiding routine that would operate on the 2MASS images, but stochastic effects made this difficult. Instead, a specific list, based on visual inspection of the 2MASS images, was made of GCs which might have centers in error by more than 2 arcsec from their nominal values. Only those GCs for which the entire distribution of IR light appears shifted with respect to the nominal optical center are listed. GCs with an asymmetric distribution of the brightest giants within 1 core radius around the optical center such as NGC 5927 and NGC 6712 are not included here;

The art of determining the location of the center of light for a GC is not trivial. We will demonstrate later that small errors of  $\sim 4$  arcsec in cluster center position are probably common in the H96 database, as was also found by Noyola & Gebhardt (2006) who analyzed archival HST images of the central regions of 38 Galactic GCs.

The new positions we thought might be appropriate for the centroids of eight GCs were carried along as additional clusters in the analysis and are listed in Table 1; a few additional cases of apparent centroid error are given in the last part of the table. For example, NGC 6541 has a central position in the 2003 version of the database of Harris (1996) which is more than  $12'$  away from its true location. The differences in  $K_s$  and in  $J - K_s$  for these small shifts for the 8 GCs are given in the fifth and sixth columns of this table. The resulting change in total brightness for these small differences in adopted GC central position can reach  $\sim 0.15$  mag, which would directly affect an optical-IR color such as  $V - K$ . The shift in a 2MASS-2MASS color such as  $J - K_s$  is smaller. The position for the cluster center adopted here for the 8 GCs listed in the first part of this table is that which gave the larger signal at  $J$ ,  $H$  and  $K_s$ .

## 2.2. Eliminating Bright Field Stars

The field star background is major concern, especially for the GCs seen against the Galactic bulge. While one could produce a CMD for the entire field of the mosaic image of a GC and then eliminate stars that do not lie along the expected cluster isochrone, we chose to adopt a scheme which is much easier to implement yet still succeeds in eliminating most of the brightest field stars. We calculate the  $K$  magnitude of the RGB tip for each cluster from its known distance and interstellar reddening assuming  $M_K(tip) = -5.9$  mag. We then add a buffer of 1.5 mag<sup>3</sup>. Stars brighter than this  $K$  are too bright to be cluster members. They were identified in the field of each GC from the 2MASS Point Source Catalog. The  $K_s$  band was used to select non-members; point sources that were deemed non-members in the  $K_s$  band were also removed in the J and H bands. A 5 x 5 pixel area around such stars was deleted from the mosaiced image for sources fainter than  $K_s = 10$ , while for brighter stars, an area 11 x 11 pixels was deleted. This cleaning operation could not be carried out close to the core of the GC where there might be crowding, which region is larger than expected due to the low spatial resolution of 2MASS, so we only selected and eliminated such sources for  $r > 0.3r_t$ .

The uncertainty in the surface brightness for each  $r_{eff}$  was the rms dispersion of the 8 sector values divided by two, taken in quadrature with the dispersion of the background measurements from the set of frames for a given cluster. The factor of two instead of  $\sqrt{8}$  reflects the difference between  $\sigma$  around a median instead of a mean (see, e.g. Lupton 1993).

## 2.3. Fitting the IR Surface Brightness Profiles

For each GC, the empirical King profile (King 1962) is fit to the surface brightness profile we determined for each of the colors  $J$ ,  $H$  and  $K_s$ . We note that this formula is distinct from the dynamical King models (King 1966a), which were used in deriving the structural parameters in TKD95 and H96; however, for the purposes of the present paper, the effective differences are expected to be sufficiently small in the radial range of interest so as to be neglected. Since the values for the  $r_t$  and GC center positions are adopted from the current version of the on line database of Harris (1996), the remaining free parameters for which we solve are the central surface brightness ( $A_0$ ) and the core radius ( $r_c$ ) for each color. The fitting procedure to determine the surface brightness uses a weighting scheme for each point (i.e. each value of  $r_{eff}$ ) based on its uncertainty, and returns the value of each of the two parameters and an error for each. The Levenberg-Marquardt fitting algorithm was used as implemented in IDL taken from <http://cow.physics.wisc.edu/~craigm/idl/down/mpfit.pro>. All the codes required to determine the surface brightness profiles and to fit them were written by SH in IDL.

---

<sup>3</sup>If we were doing this again, we would use a smaller value for the buffer.

The minimum detection for a GC to be included here is a central surface brightness of at least 10 DN above the background with a clean detection in each of the first four annuli in each of  $J$ ,  $H$  and  $K_s$ . Of the 150 GCs in the current on-line version of Harris (1996), 105 are included in our sample.

Fig. 1 shows our derived surface brightness profiles for the 30th brightest and 30th faintest GCs in our sample at  $J$  and at  $K_s$ . The fit King profile is superposed.

## 2.4. The Optical Surface Brightness Profiles

We matched our IR surface brightness profiles derived from 2MASS images onto optical ones to construct such colors as  $V - K_s$ . The surface brightness profiles at  $V$  were taken from the literature. The primary source is TKD95. They have carried out an analysis of the extensive material collected by the Berkeley Cluster Survey (see, e.g. Djorgovski & King 1986), as well as compiled many other sources of optical photometry, particularly Peterson (1986). They then fit the homogenized set of data for each GC with a grid of single mass, isotropic, non-rotating King (1966a) models. Values of  $r_c$ ,  $r_t$  and central surface brightness appropriate for the  $V$  filter were taken from their Table 2 when available. The resulting King profile was then integrated out to the desired radius to obtain the integrated light at  $V$  for a specified aperture. If there was no data for a specific GC in TKD95, but the required parameters were given in the on-line compilation database of Harris (1996), the values there were used. Nine of the GCs in our sample do not have a  $V$  surface brightness profile considered accurate from either of these two sources.

For all definite or possible core-collapsed GCs as listed in Table 2 of TKD95, we use the Chebyshev polynomial fits to the  $V$  surface brightness profile whose coefficients are given in Table 1 of TKD95. Certain key information about how to use these Chebyshev and polynomial fits to the observed surface brightness as a function of radius is missing from TKD95 as published, as are the extensive and useful notes to their Table 2. These were kindly provided to us by S. Trager and are now available through a link on his home page, see [http://www.astro.rug.nl/~sctrager/globs/cheb\\_transform.txt](http://www.astro.rug.nl/~sctrager/globs/cheb_transform.txt) and [table2notes.txt](#). Even with the aid of his notes, it was still difficult to make proper use of the Chebyshev polynomial fits, and for 61 of the GCs in our sample, including all of the core-collapsed ones, aperture photometry was carried out by integrating the measurements of the compiled  $V$  surface brightness profiles given in Table 1 of TKD95 (available through the on line edition of the AJ) to derive integrated  $V$  magnitudes. A few GCs have surface brightness profiles in this table from TKD95 with an arbitrary photometric zero point; these were ignored.

The optical surface brightness profiles for Galactic GCs are dependent on a compilation of measurements from many different programs carried out by many different groups utilizing different telescopes, instruments, filter sets, standard star fields, etc. Their zero points are based on assuming photometric sky conditions prevailed at some particular time. They do not have the all-sky uniformity of the photometric zero points which 2MASS has. This critical difference means

that the errors of any  $V$  surface brightness profile for the brighter GCs derived from reasonably deep digital (i.e. CCD) image are dominated by the uncertainty in its photometric zero point, not by random statistical measuring errors, centering errors, or stochastic errors from the finite number of very bright stars near the RGB tip.

## 2.5. The Core Radii

In our initial implementation, the core radii of the King profiles were derived independently from the fit to each of the three filters  $J$ ,  $H$  and  $K_s$ . Fig. 2 shows the difference between the  $r_c$  deduced for various pairs of filters divided by the uncertainty of this difference as a function of the core radius of each GC at  $V$ . A minimum uncertainty of 1.0" was assumed for each of the  $r_c$  (including that of  $V$ , whose uncertainty is not easily available from published material). The largest differences (in units of  $\sigma$ ) occur among the core-collapsed clusters (circled in the plots), where the optical  $r_c$ , determined from material with better spatial resolution, are typically only a few arcsec, and are always smaller than the IR  $r_c$  values. There is excellent agreement among the core radii determined from the various IR filters. The lower right panel illustrates this for the  $J$  and  $K_s$  filters; the difference for each GC between  $r_c(J)$  and  $r_c(K_s)$ , normalized by the appropriate  $\sigma$ , is shown there.

The uncertainties in  $r_c$  as listed in Table 2 are typically a few arcsec, and adaption of the independently determined  $r_c$  for each of  $J$ ,  $H$  and  $K_s$  led to unsatisfactory results, including, for example, the presence of many outliers in a plot of  $J - K_s$  colors versus  $[\text{Fe}/\text{H}]$ . The core collapsed GCs were among the worst of the outliers, as might be expected given their small  $r_c$ . In view of the excellent agreement among  $r_c(J)$ ,  $r_c(H)$  and  $r_c(K_s)$  for each cluster, we decided to tie the IR values of  $r_c$  together. The set of  $r_c$  values determined from the  $J$  mosaics of each GC are presumably the most accurate among the three IR colors; the sky is much darker than at  $H$  or  $K_s$ , while the central surface brightness at  $J$  of each GC is only slightly smaller than in the other two IR filters. In addition, the stochastic effects are smaller at  $J$  than in the redder filters. We thus set the  $H$  and  $K_s$  core radii to the value obtained from the  $J$  mosaic of each GC.

## 3. The Adopted $[\text{Fe}/\text{H}]$ Values

We adopt as our primary source of metallicities the recent homogenized compilation by Kraft & Ivans (2003) of values for  $[\text{Fe}/\text{H}]$  for Galactic GCs based on detailed analyses of Fe II lines from high dispersion spectra of individual red giants. In particular, we adopt the values given in the last column of their Table 7, based on Kurucz model atmospheres without overshoot (Kurucz 1993; Castelli, Gratton & Kurucz 1997)<sup>4</sup>. The deduced Solar Fe abundance for the work of Kraft &

---

<sup>4</sup>Grids of Kurucz model atmospheres can be downloaded from <http://kurucz.harvard.edu/grids/html>.

Ivans (2003) is  $\epsilon(\text{Fe}) = 7.52$  dex. They include values based on observations of the IR Ca triplet in individual GC red giants by Rutledge *et al.* (1997), transformed onto their system, assuming a linear transformation applies.

There are still very few accurate determinations of metallicity for the most metal rich Galactic bulge clusters. We adopt the results of Cohen *et al.* (1999) and Carretta *et al.* (2001) for NGC 6553 and for NGC 6528, the archetypical populous metal-rich bulge GCs with the smallest (but still high) reddening values. There are two other GCs in our sample with  $[\text{Fe}/\text{H}] > -0.2$  dex, Terzan 5 and Liller 1. Their adopted high metallicities are taken from Harris (1996); neither is included in the compilation of Kraft & Ivans (2003). Origlia, Rich & Castro (2002) and Origlia & Rich (2004), who analyzed high resolution near IR Keck spectra for luminous giants in Liller 1 and in Terzan 5, confirm the very high metallicity of both of these GCs. The moderate resolution IR spectroscopy of individual red giants in Liller 1 by Stephens & Frogel (2004) also supports a very high metallicity for Liller 1.

All of the GCs in the Kraft & Ivans (2003) compilation with metallicities higher than that of 47 Tuc or M71 are in fact from Rutledge *et al.* (1997). The (high) Fe-metallicities we have adopted above for NGC 6528 and NGC 6553 then suggest that the relationship between IR Ca triplet line strength (the  $W'$  parameter of Rutledge *et al.* 1997) and  $[\text{Fe}/\text{H}]$  becomes non-linear at high  $[\text{Fe}/\text{H}]$ , contrary to the assumption made by Kraft & Ivans (2003). Of the high-metallicity GCs incorporated into the compilation in this way, only NGC 6304 is probably affected (its  $[\text{Fe}/\text{H}]$  being underestimated) at a level exceeding 0.1 dex.

Results from the extensive program of Carretta & Gratton (1997), including high dispersion analyses of a sample of 24 Galactic GCs, are not incorporated into the compilation of Kraft & Ivans (2003). Carretta & Gratton (1997) studied only one GC with  $[\text{Fe}/\text{H}] > -0.7$  dex not already included in the more extensive compilation of Kraft & Ivans (2003), NGC 6352; their derived  $[\text{Fe}/\text{H}]$  is within 0.05 dex of that from Harris (1996). Kraft & Ivans (2003) do not include NGC 5272 (M3) in their compilation. We adopt  $[\text{Fe}/\text{H}](\text{FeII})$  from Cohen & Melendez (2005), adjusted for the difference in  $\log\epsilon(\text{Fe})$  for the Sun, of  $-1.36$  dex.

For the 64 GCs in our sample with no entry in the Kraft & Ivans (2003) compilation or not specifically discussed above, the  $[\text{Fe}/\text{H}]$  values given in the current on-line database of Harris (1996), which are primarily from Zinn & West (1984), are adopted. The  $[\text{Fe}/\text{H}]$  values we adopt and their sources are given for each GC in Table 3.

#### 4. Forming the Colors

We use the values of  $E(B - V)$  values given in H96 to remove the interstellar extinction. We adopt the reddening curve of Cardelli, Clayton & Mathis (1989),  $A/E(B - V) = 3.10, 0.90, 0.58$  and  $0.37$  for  $V$ ,  $J$ ,  $H$ , and  $K_s$  respectively. Integration of the King profile fits out to a specified radius for each filter  $VJHK_s$  then produces the integrated light magnitudes of the Galactic GCs.



As discussed above, due to problems in using the TKD95 polynomial fits, we directly integrated the observed  $V$  surface brightness measurements in many cases. We also ended up doing this for the IR colors as well for most of the GCs in our sample, as we will see below.

We divide the sample of Galactic GCs into three groups based on reddening and on the accuracy of the central surface brightness at  $K_s$  of the fit King profile. The “best” group has  $\text{SNR}(K_s) > 10$  and  $E(B - V) < 0.4$  mag for  $V - K$ . A larger reddening can be tolerated for  $J - K_s$  while still introducing a fixed maximum uncertainty in the color due to the much lower sensitivity of this color to a change in  $E(B - V)$ . Taking into account the size of the range in color as well as the dependence of reddening on wavelength, we adopt a cutoff in  $E(B - V)$  of 1.0 mag for  $J - K_s$ . The “fair” group has, for both of these colors, the SNR limit reduced to 5. The total sample studied here is 105 Galactic GCs; the number in each group is given in Table 4.

Since the values of  $r_c$  and  $r_t$  are fixed for  $J$ ,  $H$  and  $K_s$ , the photometric errors in IR-IR colors can be calculated directly from the uncertainties in the central surface brightness (SB) found from the King profile fits and the uncertainties in the background values. This ignores other sources of errors such as an incorrect choice of  $E(B - V)$ . If we assume a 20% uncertainty in  $E(B - V)$ , then an uncertainty in  $J - K_s$  of 0.1 mag results when  $E(B - V) = 2.1$  mag; the reddenings of 5 of the GCs in our sample exceed that value. The centroiding error is less important, since the same center was adopted for each of  $J$ ,  $H$  and  $K_s$ .

This straightforward error calculation of the photometric errors leads to substantial uncertainties for 2MASS – 2MASS colors for the fainter GCs. The  $A_0$  values deduced from the King profile fit are subject to centroiding and stochastic problems, which increase the dispersion among the 8 sectors in each radial annulus. This increase in  $\sigma$  increases the uncertainty in the derived  $A_0$ , and hence the calculated uncertainty for the IR-IR colors. Given the small range in IR-IR colors such as  $J - K_s$ , an uncertainty larger than 0.1 mag is highly undesirable. For those GCs with  $\sigma(J - K_s) > 0.15$  mag as calculated from the King profile fit parameters, we therefore bypassed the King profile fits and instead directly integrated our own measured SB profiles from the 2MASS images in  $J$ ,  $H$  and  $K_s$  out to the desired radius of 50” rather than integrating the fit King profile. This is equivalent to aperture photometry with some censoring of the data to eliminate bright non-cluster members. In the end, this was done for essentially all (104) of our sample of Galactic GCs. We used the means for the central two annuli, and the medians for the outer annuli, so as to eliminate bright field stars. The uncertainties from statistical fluctuations in measurements in any 2MASS – 2MASS color then become much smaller, as many pixels contribute to each measurement. Thus the SNR limits of 10 and 5 adopted for the “best” and the “fair” samples actually correspond to much larger values of SNR. Maximum errors in  $J$ ,  $H$  and  $K_s$  using direct integration become 0.15, 0.15 and 0.21 mag respectively.

Colors and their uncertainties for an aperture with a radius of 50” are given in Table 3. IR colors based on 2MASS images cannot be determined accurately for apertures much larger than the 50” radius adopted here due to the modest depth of these images. All colors in this table are

reddening corrected and on the 2MASS system. There are no blue outliers; i.e. there are no GCs in our sample with  $(V - K_s)_0 < 1.7$  mag. Only two of the GCs in our sample are red outliers, with  $(V - K_s)_0 > 4.3$  mag; they lie beyond the maximum  $(V - K_s)_0$  displayed in all our figures. They are Ton 2 and Djorg 1, both of which have  $E(B - V) > 1.0$  mag and neither of which can be regarded as well studied GCs with accurately determined metallicities or reddenings.

The uncertainties in IR–IR colors derived from measurement of 2MASS images that are obtained via direct integration of our SB profiles are small as the expected random (assumed Gaussian) fluctuations in measurement are small and the all-sky calibration of 2MASS photometry eliminates errors in the photometric zero point. However, many more terms make substantial contributions to the uncertainties in optical–IR colors such as  $V - K_s$  in addition to the expected random (assumed Gaussian) fluctuations in measurement. Optical–2MASS colors are seriously affected by non-random errors specific to each GC such as incorrect zero points for the  $V$  photometry, incorrect choice of reddening, or perhaps to a smaller extent inconsistent choice of the adopted cluster center for the two filters forming the color. We consider the contributions to the uncertainty in an optical–IR color of two of these in detail.

A check was made to determine how prevalent small errors for the GC center locations taken from H96 might be. We looked in the range of values of the background-subtracted amplitudes for the 8 sectors in the inner two annuli of each GC, establishing the ratio ( $R$ ) of the maximum to the minimum value in each color and checking the position angle of the sector that gave the maximum value of  $R$ . About 2/3 of those checked with adequate signal level (more than 100 DN in each color in each sector of the central two annuli) showed systematic evidence for a centroiding error, with  $R > 1.4$  for at least 4 of the 6 possible combinations of filter and annulus, and in addition showed agreement in the sector position angle which gave the maximum signal between the first and second annulus for at least two of the three filters. It is highly unlikely that contamination by field stars could produce this in regions including and so close to the GC center. Sampling (stochastic) errors can also be ruled out as the culprit as even some of the brightest GCs showed this. We therefore suspect that small errors of a few arcsec in the published centroid location of Galactic GCs are common. Examples of the implications of such positional inconsistencies on the derived magnitudes and colors are shown in Table 1. The GCs included in that table are just those that early in the course of this analysis we happened to notice might have centroiding problems. We see that for two choices of cluster center location separated by  $\sim 5$  arcsec integrating the fit King profiles produces changes in optical–IR colors reaching 0.2 mag (only up to 0.1 mag for IR–IR colors), while integrating the IR SB directly produces changes which are generally smaller for both the integrated IR magnitude and the IR–IR colors. This is another reason why we decided to use direct integration in preference to integrating the fit King profile.

The second error source we consider in detail is potential stochastic effects due to the small number of stars near the tip of the RGB, which dominate the light in the IR. This error term will be larger for optical–IR colors than for IR–IR colors. It is larger for more metal-rich GCs, with their very cool and red stars near the RGB tip, than for metal-poor GCs. We assume that photometric

contamination from non-members has been largely eliminated by the use of the sector median for annuli with  $r_{eff} > 10''$ , an assumption which may not be valid for faint clusters at low galactic latitude, for which most of the light may come from within  $10''$ . Here we evaluate the potential stochastic error in  $V - K$  arising from cluster members using the relationship for sampling errors of King (1966b) and the luminosity function of M3. The  $V$  band luminosity function is from Sandage (1957), while  $V - K$  colors along the isochrone are taken from the grid of Girardi *et al.* (2002). At a total luminosity of 1% that of M3, the sampling error ( $E$ ) in  $V - K$  is 0.06 mag. The fractional sampling error for each GC is then  $E \propto \sqrt{\frac{L(M3)f(M3)}{Lf}}$ , where  $f$  is the fraction of the total light in the aperture of interest. For the GCs studied here and with our adopted aperture radius of  $50''$ , the sampling error in  $V - K$  ranges up to 0.15 mag; the value for M3 itself is 0.01 mag. This term will dominate the V-IR color error in a few cases, and will be comparable to the probable  $V$  photometric zero point uncertainty error in additional cases.

Many other factors may also contribute to the optical-IR color uncertainties for GCs. For those clusters with large  $E(B - V)$ , the reddening will surely be patchy over the face of the GC (see. e.g. Cohen & Sleeper 1995). Application of standard reddening corrections with any adopted effective  $E(B - V)$  cannot accurately reproduce the true reddening corrections of such objects. For the GCs with very high background stellar density, such as those seen against the Galactic bulge, the issue of field star contamination may become important, although we have taken a number of steps to minimize this. It should also be noted that we have assumed circular isophotes, a valid assumption for most GCs. White & Shawl (1987) find that only 32% of Galactic GCs are flatter than  $b/a < 0.9$  and 5% are flatter than 0.8 (NGC 6273 being the flattest of their sample of 100 GCs, with  $b/a = 0.73$ ), so on the whole the Galactic GCs are quite round.

Bearing all this in mind, we ascribe to optical-IR colors uncertainties of 0.20 mag for the “best” sample, and 0.25 mag for the “fair” sample of GCs considered here. Even larger uncertainties seem appropriate for the remaining GCs due to their high reddenings.

Fig. 3 and 4 show the reddening corrected  $(V - K_s)_0$  and  $(J - K_s)_0$  colors as a function of  $[\text{Fe}/\text{H}]$  for the sample of “best”, “fair” and all included GCs. The “best” sample is shown as large filled circles in the upper left panel. Smaller filled circles are used in the other two panels to denote those GCs in the “fair” sample not included in the “best” sample, while those not included in the “fair” sample are shown in the lower left panels as small open circles. The  $J - K_s$  plot shows a very good relationship, with small scatter. Even the plot in the lower left panel including all 105 GCs in our sample looks quite good. The outlier in the “fair” sample is HP 1, which has a high uncertainty in  $J - K_s$  and lies  $\sim 2.5\sigma$  higher than typical for its  $[\text{Fe}/\text{H}]$ . But in a sample this large, one such outlier might be expected, and in addition this GC can hardly be considered a well studied cluster with an accurately determined reddening or metallicity.

The  $V - K_s$  plot (Fig. 3) has a much larger vertical scale than does Fig. 4. The relationship between  $(V - K_s)_0$  and  $[\text{Fe}/\text{H}]$  is good, but, not surprisingly, shows a significantly larger dispersion than that of  $(J - K_s)_0$  versus  $[\text{Fe}/\text{H}]$ . The lower left panel displaying the 96 GCs with photometrically

calibrated  $V$  SB profiles has a very large  $\sigma$  due in part to the high  $E(B - V)$  values of some of the GCs included here. None of the four GCs in our sample with  $[\text{Fe}/\text{H}] > -0.2$  dex is included in the “best” or “fair”  $V - K_s$  sample; they each have reddenings that exceed the cutoff value.

### 5. Fits to V-J, V-H, V-K and J-K as Function of $[\text{Fe}/\text{H}]$

We fit various  $V$ –IR and IR–IR 2MASS reddening corrected colors as a function of  $[\text{Fe}/\text{H}]$ . Quadratic fits are given for  $V - J$ ,  $V - H$ ,  $V - K_s$ ,  $J - H$  and  $J - K_s$ . Linear fits are given when there is little improvement between the linear and second order fits. A fit for the “best” and for the “fair” samples are carried out for each color. The coefficients for these fits are given in Table 8 as are the rms dispersion about each fit of the sample GCs. An augmented “fair” sample was created, which additionally contains all of the four GCs in our sample with  $[\text{Fe}/\text{H}] > -0.2$  dex. This requires adding three GCs to the  $V - K_s$  “fair” sample (Liller 1 does not have a calibrated  $V$  surface brightness profile, hence no  $V - K$  color). Two GCs (Terzan 5 and Liller 1) must be added to the sample for  $J - K_s$ . The uncertainty in  $(V - K_s)_0$  is taken as 0.5 mag for Terzan 5, given its high reddening, and is set to 0.3 mag for the other two added GCs. Uncertainties for the four GCs with  $[\text{Fe}/\text{H}] > -0.2$  dex in  $(J - K_s)_0$  are assigned as a sum in quadrature of the photometric error and the consequence of a 10% uncertainty in  $E(B - V)$ . Fits for the augmented sample in each color (also given in Table 8) enable us to probe the behavior of the colors in the regime near Solar metallicity.

Linear fit are adequate for all  $V$ –IR colors unless the very high  $[\text{Fe}/\text{H}]$  GCs are added, at which point quadratic fits are clearly superior. Linear fits suffice for the IR–IR colors of the GCs in the “best” sample. But the quadratic term is statistically significant for the  $J - K_s$  “fair” sample, which already contains two of the four highest metallicity GCs.

The dispersions around the fit of the measured IR–IR 2MASS colors  $J - K_s$  and  $J - H$  are small and only slightly larger than the expected assuming Gaussian statistical variances of measurement for the observed signal levels. Thus the many other potential sources of error are not of great significance for these specific colors. The rms dispersion around the fits to the  $V$ –IR colors suggests typical total uncertainties in the  $V$  integrated light of  $\sim 0.25$  mag, in good agreement with the estimates discussed above for the many terms contributing to the total error.

The luminosity function for the Galactic globular cluster system at  $K_s$  has been formed by combining our  $(V - K_s)_0$  colors with the total absolute  $V$  mags from the database of H96 for those GCs in our sample with  $E(B - V) < 0.4$  mag. For the remaining GCs, the fits to  $V - K_s$  as a function of  $[\text{Fe}/\text{H}]$  given in Table 8 have been used to predict the integrated light color from the Fe-metallicity of each GC (taken from H96). All 146 GCs from the H96 database which have total  $M_v$  tabulated there are included. There are perhaps another 5 known Galactic GCs, all of which are extremely reddened and poorly studied. Fig. 5 shows the resulting  $K_s$  luminosity function, which is peaked at  $M(K)_0 \sim -9.7$  mag, or  $L \sim 1.6 \times 10^5 L_\odot$  for  $M_K(2\text{MASS}) = 3.29$  mag, and

(adopting  $M/L_K = 1.4$ ) is  $M \sim 2.2 \times 10^5 M_\odot$ .

## 6. Comparison with Other Studies

### 6.1. The 1977 Data of Aaronson, Malkan & Kleinmann

The only previous substantial body of photometry of the integrated light of Galactic GCs in the IR is the work of Aaronson, Malkan & Kleinmann in the late 1970s. A brief description of their data is given in Aaronson, Cohen, Mould & Malkan (1978), where the data was used in a number of plots. However, due to M. Aaronson’s tragic and untimely death, the data was never published in full<sup>5</sup>. We do so here in Table 5, recognizing again that this is the data of Aaronson, Malkan & Kleinmann as it existed in 1978. They observed the central regions of 54 GCs using a single channel photometer on the KPNO No. 1 0.9m telescope with a beam size whose diameter in most cases was 105”. Background corrections were made chopping to fields  $\sim 200''$  away. Integration times were set to achieve a photometric accuracy of  $\leq 0.02$  mag for  $J$ ,  $H$  and  $K$ . Narrow band indices measuring the absorption in the  $2.4\mu$  CO band and in the  $1.9\mu$  H<sub>2</sub>O band were obtained as well for some of these GCs. They combined these with optical surface brightness profiles from the literature as it existed at that time to derive  $V - K$  colors as well. It is important to note that they used a smaller telescope than did 2MASS, with a now obsolete and noisy single channel detector, but with longer integration times. They divided their final sample into 14 calibrating GCs, whose reddenings and metallicities were believed to be well known, 23 other GCs, which were believed to be useful, and 27 GCs with only one or two measurements, regarded as less reliable, which were not used in Aaronson, Cohen, Mould & Malkan (1978).

Two versions of this old data exist. The first is a list of the observed colors, preserved by M. Malkan from about 1977 and recovered from old computer files. These are the values given in Table 5. The observed broad band colors are listed, while the reddening corrected CO and H<sub>2</sub>O indices are tabulated. The reddening corrections for the narrow band indices are very small as the wavelength range covered in these measurements is very narrow. Frogel, Persson & Cohen (1979) use  $E(CO)/A_V = -0.007$ <sup>6</sup> and  $E(H_2O)/A_V = 0.019$  mag, so any difference between the  $E(B - V)$  values adopted in 1978 versus those in current use has a negligible effect. The second archive of these integrated light GC observations is a list preserved in a notebook from 1977 of the dereddened values used by J. Cohen to generate the figures and fits presented in Aaronson, Cohen, Mould & Malkan (1978). These values agree well with those in M. Malkan’s archive for  $J - K$  (the mean difference for 37 GCs is 0.01 mag, with  $\sigma = 0.04$  mag) with somewhat larger differences in  $V - K$  (mean difference for 35 GCs is 0.04 mag, with  $\sigma = 0.11$  mag). It is believed that these differences

---

<sup>5</sup>The data from M. Aaronson and M. Malkan tabulated in Brodie & Huchra (1990) were unofficial preliminary values for a subset of the clusters included in the 1978 study.

<sup>6</sup>The reddening corrected CO indices are larger than the observed ones.

arise from the slightly different values of  $E(B - V)$  and in the mean colors used in 1977 during the preparation of the manuscript for Aaronson, Cohen, Mould & Malkan (1978) versus those adopted and archived by M. Malkan at the end of all relevant observing runs and reduction thereof in 1979. The four GCs with  $\Delta(V - K)$  exceeding 0.20 mag between the two independent archives are marked in the table. The nominal errors of these measurements, excluding the 27 considered less reliable, henceforth ignored here, are  $\pm 0.15$  mag for  $V - K$  and  $\pm 0.04$  mag for  $J - K$ .

In order to compare our colors derived from 2MASS and those of Aaronson, Malkan & Kleinmann as they existed in 1978, we transform the observed colors recorded by M. Malkan from the CIT system to which we believe the measurements were calibrated<sup>7</sup> into that of 2MASS using the equations in §4.3 of Carpenter (2001).

We show in Fig. 6 our “best” and “fair” samples in the reddening corrected colors  $(V - K_s)_0$  and in  $(J - K_s)_0$  as a function of cluster Fe-metallicity with the results of Aaronson, Malkan & Kleinmann superposed. Current values for the reddening and metallicity for each GC are used with the 1977 observed colors in this figure. The range of GC colors is much smaller in  $(J - K_s)_0$  than it is in  $(V - K_s)_0$ ; the scale of the Y axis of the upper panel of Fig. 6 is correspondingly much larger than that of the lower panels. The differences are shown as functions of our derived 2MASS colors in Fig. 7; some statistics of these differences are given in Table 6. Observed colors are compared here; the choice of  $E(B - V)$  and of metallicity for each GC is irrelevant. This table shows that the dispersion in the differences for  $V - K_s$  as measured in 1977 (transformed into the 2MASS system) and our measurements is consistent with the errors, and the means agree to within the uncertainties of the measurements. For  $J - H$  and  $J - K_s$ , the dispersion in the differences between the colors of Aaronson, Malkan & Kleinmann 1977 photometry (transformed into the 2MASS system) and our colors is small, only 0.07 mag, easily consistent with the measurement uncertainties for the two data sets. However, there is a small systematic offset, apparent in both Table 6 and in the lower panels of Fig. 7, of 0.13 mag such that the 1977 colors are systematically redder in  $J - K_s$  and in  $J - H$  than our colors. This does not appear to be function of  $J - K_s$ , but rather a constant offset.

We ascribe these systematic offsets in the IR–IR colors between the 1977 data and the present set, at least in part, to the difficulty of tracing now exactly how the 1978 measurements were calibrated and of transforming between the various photometric systems involved. The  $J$  filter adopted by the 2MASS project is somewhat broader than most other  $J$  filters, extending into the adjacent blue and red  $H_2O$  absorption bands; see the discussion in Carpenter (2001), who has derived relationships between the many flavors of  $JHK$  in use and the filter set adopted by 2MASS, and in Cutri *et al.* (2003). When one examines the range of the coefficients for transforming various types of  $J - K$  colors into the 2MASS system over the full suite of IR photometric systems in use, one concludes that it might be possible to explain the small systematic offsets seen in the lower panels Fig. 7 and in Table 6 for  $J - K_s$  and for  $J - H$  as errors in the coefficients of the transformation equation we used. The definition of the  $H$  and of the  $K$  filters are more consistent

---

<sup>7</sup>We thank the referee, John Huchra, and Jay Frogel for confirming that the CIT system was used.

between the various IR photometric systems in use than that of  $J$  and hence  $H$  or  $K$  magnitudes are less subject to such transformation uncertainties.

The coefficients of the fits to  $V - K$  and  $J - K$  versus  $[\text{Fe}/\text{H}]$  derived by Aaronson, Cohen, Mould & Malkan (1978) in 1977 (transformed into 2MASS colors) from their small sample of calibrating GCs (only 14 clusters) are included in Table 8. A comparison of these linear fits with those to the “best” present measurements versus  $[\text{Fe}/\text{H}]$  shows excellent agreement in both cases, as should be expected given the agreement between the two data sets shown in Fig. 6. The constant coefficients for  $J - K_s$  differ by only 0.03 mag, well within the errors of the 1977 fit, with the 1977 data being slightly redder for a fixed  $[\text{Fe}/\text{H}]$ , as expected from the discussion above.

Given the uncertainties of the Aaronson, Malkan & Kleinmann data and of the present colors derived from 2MASS images, the agreement overall is very good for  $V$ –IR(2MASS) and reasonably good for IR–IR colors. We have demonstrated that the measurements of integrated light colors of Galactic GCs carried out by Aaronson, Malkan & Kleinmann in 1977 appear to be valid and to agree reasonably well with our current measurements based on 2MASS images. This suggests that the overlap found by Frogel, Persson & Cohen (1980) between the integrated light colors of the M31 GCs and those of the Milky Way GCs is also still valid. This might not hold for the expanded set of objects today considered to be GCs in M31, but see the discussion regarding the reliability of identifications of purported “young GCs” in M31 by Cohen, Matthews & Cameron (2005).

## 6.2. The Work of Nantais *et al.* (2006)

Very recently Nantais *et al.* (2006) present a compilation of infrared light photometry for 96 Galactic GCs generated using aperture photometry for diameters from 7 to 70 arcsec on 2MASS images. This was combined with integration of the optical surface brightness measurements of Peterson (1986) to create  $V - K_s$  colors. Of these only 68 were considered reliable, the remainder having problems in the matching of the optical and IR photometry. A comparison of our results with theirs is shown in Fig. 8 for the sample in common, with statistics of the differences given in Table 7. Those with  $V - J < 0$ , considered not “reliable” by Nantais *et al.* (2006), were excluded. They also exclude those with  $V - J < V - I$ ; J. Nantais kindly supplied a list of those GCs excluded as not “reliable”.

Figure 8 illustrates the differences in the two sets of colors for the integrated light of Galactic GCs. The agreement in the mean for these two data sets for the pure IR colors, i.e.  $J - K_s$  or  $J - H$ , is excellent and the dispersion of the set of differences (0.12 mag) is consistent with the photometric errors we have calculated (given in Table 3). Since both sets are based on 2MASS images, this agreement, while gratifying, is only to be expected. A comparison of the two sets of  $V - K_s$  colors for the objects in common, however, shows a very large mean difference of 0.63 mag (ours being on average redder) and a very large dispersion ( $\sigma = 0.52$  mags). This is quite unlike the comparison of our  $V - K_s$  colors for Galactic GCs with those of Aaronson, Malkan & Kleinmann

from 1977; compare the upper left panel of Figure 8 with that of Figure 7 and note the much larger range of  $V - K_s$  shown in the latter figure. Our  $V$ –IR colors have been derived with some care and are in good agreement with those of Aaronson, Malkan & Kleinmann from 1977. We believe that they are more reliable than those of Nantais *et al.* (2006).

## 7. Color Gradients Within Globular Clusters

Color gradients within  $1r_c$  of the center of a GC can arise due to stochastic effects of the small number of luminous giants dominating the IR light. If these are by chance not symmetrically distributed about the true center of the total integrated light of the GC, a distortion of the central position will occur. This will result in a small central region which is apparently redder and more luminous than expected based on the cluster surface brightness profile over a large radial range. For sparse clusters, there may be a statistical fluctuation in the distribution of the most luminous red giants such that there is no such star close to the location of the optical center; a center bluer than the integrated cluster light would then occur. However, we are interested here in possible larger scale intrinsic gradients of the cluster light. While our data are not ideal for this purpose given the short exposures and relatively shallow depth of the 2MASS images, we explore this issue.

Our analysis suggests that  $r_c$  is the same for each of  $J$ ,  $H$  and  $K_s$  to within the errors, as is demonstrated for  $J$  and  $K_s$  in the bottom right panel of Fig. 2. We have explicitly assumed in the construction of the surface brightness profiles for  $J$ ,  $H$  and  $K_s$  from 2MASS frames that  $r_t$  and  $r_c$  are fixed for each GC. This in turn implies that IR–IR colors for Galactic GCs are independent of radius, depending only on the ratio of the central surface brightness in the two colors. Furthermore, we consider the IR surface brightness profiles as uncertain at radii approaching  $r_t$ . Thus only the optical–IR colors among those considered here could potentially reveal color gradients, and those only over a radial range extending out to  $r \ll r_t$ . Given our assumptions, the existence of a color gradient in  $V$ – $J$ ,  $H$  and  $K_s$  would manifest itself in our analysis as a difference between  $r_c$  for  $V$  and that for the 2MASS filters. If  $r_c(V)$  is larger than  $r_c(J)$ , the value to which we set  $r_c(H)$  and  $r_c(K_s)$ , then the integrated  $V - J$  will become bluer as  $r$  increases over the radius range from 0 out to about  $5r_c$ , after which the color gradient is not easily detected, since  $r_t$  was assumed to be the same for all colors investigated here. If  $r_c(V)$  is smaller than  $r_c(J)$ ,  $V - J$  will become redder as  $r$  increases over that radial range.

The existence of color gradients, at the level to which we can detect them, thus depends on whether there are GCs for which  $r_c$  is not the same for  $V$  and for  $J$ . Fig. 2 shows that for most GCs, the assumption of equality is valid. This figure was constructed assuming that the error in  $r_c(V)$ , which we do not know, is  $1.0''$ . If we raise that to  $2.0''$ , then only 11 GCs may show a detectable color gradient. Several of these are probable or definite core collapsed GCs as indicated below. NGC 1904 (c?) 4833, 6266 (c?), 6397 (C), 6522 (C) and 6356 have  $r_c(V) - r_c(J) > 2.5\sigma(\Delta r_c)$ , while NGC 6333, 6584 and 7006, with the same  $2.5\sigma$  tolerance have  $r_c(J) > r_c(V)$ . Only NGC 6266 (c?) and 6397 (C) have a difference exceeding  $4\sigma$ ; these are a definite core-collapsed GC and a



probable one, so large differences in  $r_c(V)$  versus  $r_c(\text{IR})$  should be expected given the spatial resolution of the 2MASS images.

The accuracy of the set of values of  $r_c(V)$ , which we have assumed here to be high (i.e.  $\leq 2''$ ), is crucial to this argument. Yet the very recent work of Beccari *et al.* (2006), who determined an accurate  $V$  surface brightness profile for the cluster NGC 6266, demonstrates that concern with the accuracy of values of  $r_c(V)$  in compilations such as H96 is warranted. Their recent precision measurement of  $r_c(V)$  for this GC is  $19''$ , in agreement with our value of  $r_c(J)$  of  $25.6 \pm 2.9''$ , but is 30% larger than the value given by H96. This resolves one of the two cases for which a discrepancy of  $4\sigma$  or larger appears to exist between the  $V$  and IR core radius. Furthermore, although TKD95 called NGC 6266 a probable core collapsed cluster, Beccari *et al.* (2006) find that NGC 6266 is not a core-collapsed GC.

Thus, to the level at which we can detect color gradients and out to a radius  $r < 5r_c$ , no GC in our sample appears to have such, but our ability to detect radial color gradients is severely limited by the modest depth of the 2MASS images. Intrinsic large scale color gradients in GCs such as might arise from mass segregation are difficult to detect even in the best available data as discussed by Djorgovski & Piotto (1993).

## 8. Comparison with Single Burst Integrated Light Models

We next compare our results to a number of predictions from single burst simple stellar populations (SSPs) of a unique age and metallicity. There are many predicted grids of colors for SSP populations based on various stellar evolutionary codes, assumptions about the HB, the AGB, etc. We must know which photometric system was used to generate the model output colors as well as that of any photometric databases used to calibrate the model’s photometric zero points.

The specific SSP models considered here are those of Buzzoni (1989), Maraston (2005) and Worthey (1994). A somewhat larger consensus value for the age of GCs was prevalent in the astronomical community prior to 2000, so we adopted models with ages of 12 Gyr from Buzzoni (1989), while the 11 Gyr model of Maraston (2005) was selected. We follow the assumption made by Worthey (1994) of an age of 15 Gyr for Galactic GCs. These all use the IR filter transmission curves of the Johnson system. We convert their predicted colors to the 2MASS system using the transformations given in Appendix A of Carpenter (2001).

The  $[\text{Fe}/\text{H}]$  values we adopt here refer to Fe itself. No adjustment has been made for any enhancement of the  $\alpha$ -process elements, ubiquitous among GC stars. Since it is generally believed that  $[\alpha/\text{Fe}] \sim +0.3$  dex for GC stars (see, e.g. Cohen & Melendez 2005, and references therein), we use the global metallicity parameter as defined by Salaris, Chieffi & Straniero (1993) to adjust  $[\text{Fe}/\text{H}]$  to  $[\text{M}/\text{H}]$  (i.e. the parameter  $\log(Z)$  used by stellar evolution codes). Then  $[\text{M}/\text{H}] = [\text{Fe}/\text{H}] + 0.2$  dex for the  $\alpha$ -enhancement typical of GCs. Each of the three model tracks were offset by  $-0.2$  dex in  $[\text{Fe}/\text{H}]$  to compensate for their assumed scaled Solar elemental abundances.

Fig. 9 shows the three predicted SSP model tracks superposed on the “best” and “fair” GC samples; the photometric system of the displayed colors is that of 2MASS. Although for  $V - K_s$  none of the four GCs in our sample with  $[\text{Fe}/\text{H}] > -0.2$  dex is in the “fair” sample, the three of these clusters which have  $V - K_s$  colors are shown as open circles in the upper right panel. The two such GCs (Terzan 5 and Liller 1) that are not in the  $J - K_s$  “fair” sample due to their very high reddenings are similarly shown in the lower right panel with error bars representing the sum in quadrature of the photometric error and a the consequence of a 10% uncertainty in  $E(B - V)$ .

Each of the predicted SSP color-metallicity tracks overlays the  $(V - K_s)_0 - [\text{Fe}/\text{H}]$  relationship we have derived for Galactic GCs over the metal-poor regime  $[\text{Fe}/\text{H}] < -0.5$  dex. However, the lower panels of Fig. 9 show a slight offset of  $\sim 0.1$  mag at a fixed  $[\text{Fe}/\text{H}]$  such that the models are slightly redder in  $J - K_s$  than the color we derive from 2MASS. Since the agreement of our derived  $J - K_s$  colors with those of Nantais *et al.* (2006) is perfect (at the level of  $\pm 0.01$  mag), one cannot ascribe this difference to problems in our IR-IR colors.

There are two possible explanations for this offset between the SSP models and the actual colors of the Galactic GCs. Fig. 7 and Table 6 show a similar small offset between the photometry of integrated light colors by Aaronson, Malkan & Kleinmann from 1977 and the 2MASS based colors presented here in the sense that the 1977  $(J - K_s)_0$  colors transformed to the 2MASS system are somewhat redder than the ones we derive here. This is the same sign as the differences seen between the predicted SSP model colors and those we derive for Galactic GCs, and is of the same magnitude as the problem seen in the lower panels Fig. 9 for  $J - K_s$ . This should not be surprising, as the validity of such models for the integrated light of simple stellar systems as a function of metallicity and age is generally established at least in part by attempting to reproduce as a key test the integrated light colors of Galactic GCs; the ACMM colors (i.e. their fits of color as a function of  $[\text{Fe}/\text{H}]$ ) were the only ones available for this purpose prior to the present. (This does not explain the origin of the offset in  $J - K_s$  seen in the lower panels of Fig. 9; it just shifts the problem back to the details of the calibration of the Aaronson, Malkan & Kleinmann 1977 data.)

A second possibility relates to the photometric system of the calibration data. These models are all calibrated using the photometry of Frogel, Persson & Cohen (1983) and Cohen, Frogel & Persson (1983) for individual red giants in Galactic GCs, as that was the largest sample of such data available until quite recently. Most model codes utilize the Johnson filter transmission curves for  $J$  and for  $K$ , while the key 1983 data sets were calibrated to and published in the CIT system. Consider a star with a  $(J - K)_0(2\text{MASS})$  color of 0.65 mag. As observed, for a typical  $E(B - V)$  of 0.4 mag, it will have a color on the 2MASS system of 0.86 mag, and will have an observed  $(J - K)(\text{CIT})$  of 0.83 mag while  $(J - K)(\text{Johnson})$  will be 0.90 mag according to the transformation equations derived by Carpenter (2001). This star will thus be 0.07 mag redder in  $J - K$  in the Johnson system than in the CIT system. If a model code does not take these differences among the IR systems into account, errors will occur in the predicted  $J - K$  colors (in whatever IR photometric system is adopted for the output of the model) which reproduce the sign and approximate magnitude of the offset seen between the model SSP integrated light IR-IR colors

and our measured ones for Galactic GCs in the bottom panels of Fig. 9. Construction of models, as well as prediction and testing of integrated colors from them, requires careful attention to the details of the calibration of any stellar or integrated light photometry used in that process.

Only the predicted SSP  $(V - K_s)_0$  colors of Worthey (1994) reproduce the very red colors we find for Galactic GCs at metallicities between  $-0.5$  dex and the Solar value. It must be emphasized that the validity of the models cannot be probed at metallicities above Solar from this dataset, as the sample of well studied Galactic GCs with such high metallicities is small to non-existent.

For an old (age  $\sim 10$  Gyr) single-burst population, an uncertainty in color of 0.10 mag corresponds to an error in Fe-metallicity of 0.25 dex for  $V - K_s$  colors and to 0.7 dex for IR–IR colors; the latter is so large as to render any conclusion regarding the metallicity of a GC useless. The apparent mismatch between the SSP model predictions and our  $J - K_s$  colors suggests caution in using IR–IR colors to determine metallicities (or ages) for GCs in distant galaxies.

## 9. Summary

We have mosaiced 2MASS images to derive surface brightness profiles in  $J$ ,  $H$  and  $K_s$  for 104 Galactic globular clusters, incorporating algorithms to reduce the impact of bright field stars. We fit these with empirical King (1962) profiles, adopting tidal radii and cluster center positions from the literature. This leaves only the central surface brightness and the core radius as parameters to be determined. We show that the resulting core radii for each of these three IR colors are identical to within the errors. We therefore set  $r_c$  for each of  $J$ ,  $H$  and  $K_s$  to be  $r_c(J)$ . We then show that the  $r_c(J)$  for each GC are identical to the core radii at  $V$  in essentially all cases if the uncertainty for  $r_c(V)$  is taken to be  $2''$ . The only discrepant cases are core collapsed GCs, where the lower spatial resolution of 2MASS combined with the small optical core radii produce smaller measured core radii at  $V$  than in the IR from 2MASS.

We derive integrated light colors  $V - J$ ,  $V - H$ ,  $V - K_s$ ,  $J - H$  and  $J - K_s$  for these globular clusters. We do this by directly integrating the surface brightness profiles in most cases, equivalent to slightly censored aperture photometry, as this leads to smaller statistical measurement uncertainties than does integrating the fit King profiles. Each color shows a reasonably tight relation between the dereddened colors and metallicity. Fits of these are given for each color. Linear fits suffice when the most metal-rich GCs are not considered. Once the four GCs in our sample with  $[\text{Fe}/\text{H}] > -0.2$  dex are included, a quadratic fit is necessary. We use our derived  $V - K_s$  colors, combined with total  $M_V$  from the database of H96, to find the luminosity function at  $K_s$  of the Galactic globular cluster system.

The IR–IR colors have very small errors and very low dispersions about the fits due largely to the all-sky photometric calibration of the 2MASS survey. These errors are consistent with the expected random fluctuations of the measurements based solely on the measured signal levels, indicating that other sources of error do not contribute much. The  $V$ –IR colors have substantially

larger uncertainties due in part to the lack of an all-sky photometric calibration for surface brightness measurements at optical wavelengths. Incorrect choices for reddening, discrepancies in the adopted position of the center of a cluster, and, for the least populous GCs, stochastic errors due to the small number of luminous stars near the tip of the red giant branch, also contribute to the uncertainties in the  $V$ –IR colors.

We find good agreement with measurements of integrated light colors for a much smaller sample of Galactic globular clusters by Aaronson, Malkan & Kleinmann from 1977. Small constant offsets between the two datasets of  $\sim 0.1$  mag in IR–IR colors are required; we ascribe them to the difficulties of transforming between the filter and detector system used in 1977 and the 2MASS system. We find excellent agreement with the IR–IR colors of Nantais *et al.* (2006), not surprising since they too use 2MASS images from which to derive their colors. But a comparison at  $V - K_s$  of our colors with theirs shows very poor agreement in the mean, and with a very large dispersion; we suspect that they did not correctly match the optical and IR magnitudes in many cases.

Our results provide a calibration for the integrated light of distant single burst old stellar populations from very low to Solar metallicities. We compare our dereddened measured colors with predictions from several models of the integrated light of single burst old populations, bearing in mind that the models have almost certainly been set up to reproduce the data of Frogel, Persson & Cohen (1983) and Cohen, Frogel & Persson (1983) for colors of individual red giant branch stars in Galactic GCs. While there is reasonable agreement for  $V - K_s$  colors, a  $\sim 0.1$  mag offset is required in  $J - K_s$ , with the model predictions being redder than our colors. Until the origin of this problem is understood, any determination of  $[\text{Fe}/\text{H}]$  (or age) in old populations based on IR–IR colors cannot be considered valid. In addition, some of the models fail to reproduce the behavior of the integrated light  $V - K_s$  colors of the Galactic globular clusters near Solar metallicity.

This publication makes use of data products from the Two Micron All Sky Survey, which is a joint project of the University of Massachusetts and the IPAC/Caltech, funded by NASA and by NSF. We thank John Carpenter and Pat Côté, who participated in the initial phase of this work. J.G.C. is grateful to NSF grant AST-0507219 for partial support. S.H. was supported by a Summer Undergraduate Research Fellowship, provided in part through NSF grant AST-0205951 to J.G.C. S.A.M. acknowledges support from a Spitzer postdoctoral fellowship. SGD acknowledges partial support from the Ajax Foundation.

## REFERENCES

- Aaronson, M., Cohen, J. G., Mould, J. R. & Malkan, M., 1978, *ApJ*, 223, 824
- Armandroff, T. E. & Zinn, R., 1988, *AJ*, 96, 92
- Beccari, G., Ferraro, F. R., Possenti, A., Valenti, E., Origlia, L. & Rood, R. T., 2006, *AJ*, 131, 2551

- Brodie, J. P. & Huchra, J. P., 1990, *ApJ*, 362, 503
- Buzzoni, A., 1989, *ApJS*, 71, 817
- Cardelli, J. A., Clayton, G. C. & Mathis, J. S., 1989, *ApJ*, 345, 245
- Carpenter, J. C., 2001, *AJ*, 121, 2851
- Carretta, E. & Gratton, R., 1997, *A&AS*, 121, 95
- Carretta, E., Cohen, J. G., Gratton, R. G. & Behr, B. B., 2001, *AJ*, 122, 1469
- Castelli, F., Gratton, R. G. & Kurucz, R. L., 1997, *A&A*, 318, 841
- Cohen, J. G., Frogel, J. A. & Persson, S. E., 1983, *ApJ*, 275, 773
- Cohen, J. G. & Sleeper, E. C., 1995, *AJ*, 109, 242
- Cohen, J. G., Gratton, R. G., Behr, B. B. & Carretta, E., 1999, *ApJ*, 523, 739
- Cohen, J. G. & Melendez, J., 2005, *AJ*
- Cohen, J. G., Matthews, K. & Cameron, P. B., 2005, *ApJ*, 634, L45
- Cutri, R. M. *et al.*, 2003, “Explanatory Supplement to the 2MASS All-Sky Data Release”, <http://www.ipac.caltech.edu/2mass/releases/allsky/doc/explsup.html>
- Djorgovski, S. G., 1986, in *IAU Symposium 126, The Harlow-Shapley Symposium on Globular Cluster Systems in Galaxies*, eds. J. E. Grindlay & A. G. Davis Philip, (Reidel, Dordrecht), pg. 333
- Djorgovski, S. & King, I. R., 1986, *ApJ*, 305, L61
- Djorgovski, S. & Piotto, 1993, in *Structure and Dynamics of Globular Clusters*, ed. S.G. Djorgovski & G. Meylan, ASP Conf. Ser. 50 (San Francisco: ASP), 203
- Djorgovski, S. & Meylan, G., 1993, in *Structure and Dynamics of Globular Clusters*, ed. S.G. Djorgovski & G. Meylan, ASP Conf. Ser. 50 (San Francisco: ASP), 373
- Fischer, P. Welch, D. L., Côté, P., Mateo, M. & Madore, B. F., 1992, *AJ*, 103, 857
- Frogel, J. A., Persson, S. E. & Cohen, J. G., 1979, *ApJ*, 227, 499
- Frogel, J. A., Persson, S. E. & Cohen, J. G., 1980, *ApJ*, 240, 785
- Frogel, J. A., Persson, S. E. & Cohen, J. G., 1983, *ApJS*, 53, 713
- Girardi, L. Bertelli, G., Bressan, A., Chiosi, C., Groenewegen, M. A. T., Marigo, P., Salasnich, B. & Weiss, A., 2002, *A&A*, 391, 195

- Harris, W. E., (H96), 1996, AJ, 112, 1487
- King, I. R., 1962, AJ, 67, 471
- King, I. R., 1966a, AJ, 71, 64
- King, I. R., 1966b, AJ, 71, 276
- Kraft, R. P. & Ivans, I. I., 2003, PASP, 115, 143
- Kurucz, R. L., 1993, CD Rom No. 13
- Lupton, R., 1993, *Statistics in Theory and Practice*, , Princeton Univ. Press, p. 43
- Maraston, C., 2005, MNRAS, 362, 799
- Nantais, J. B., Huchra, J. P., Barmby, P., Olsen, K. A. G. & Jarrett, T. H., 2006, AJ, 131, 1416
- Newell, B. & O’Neil, E. F., 1978, ApJ, 37, 27
- Noyola, E. & Gebhardt, K., 2006, ApJ, in press
- Origlia, L., Rich, R. M. & Castro, S., 2002, AJ, 123, 1559
- Origlia, L. & Rich, R. M., 2004, AJ, 127, 3422
- Peterson, C. J., 1986, PASP, 98, 192
- Rutledge, G., Hesser, J. & Stetson, P., 1997, PASP, 109, 907
- Salaris, M., Chieffi, A. & Straniero, O., 1993, ApJ, 414, 580
- Sandage, A. R., 1957, ApJ, 125, 422
- Shawl, S. J. & White, R. E., 1986, AJ, 91, 312
- Skrutskie, M. F. *et al.*, 2006, AJ, 131, 1163
- Stephens, A. W. & Frogel, J. A., 2004, AJ, 127, 925
- Trager, S. C., King, I. R. & Djorgovski, S., (TKD95) 1995, AJ, 109, 218
- White, R. E. & Shawl, S. J., 1987, ApJ, 317, 246
- Worthey, G., 1994, ApJS, 95, 107
- Zinn, R., 1985, ApJ, 293, 424
- Zinn, R. & West, M. J., 1984, ApJS, 55, 45

Table 1. Integrated IR Colors For GCs With Two Choices for the Position of the Center

ID	RA,Dec (Harris) (J2000)	RA,Dec (2MASS) (J2000)	$\Delta\theta$ (arcsec)	$\Delta K_s^a$ (mag) (King profile int.)	$\Delta J - K_s^a$ (mag) (Direct SB prof. int.)	$\Delta K_s^a$ (mag)	$\Delta J - K_s^a$ (mag)
NGC 5824	15 03 58.5 −33 04 04	15 03 58.30 −33 04 07	3.9	0.08	−0.01	−0.01	−0.01
NGC 6553	18 09 17.6 −25 54 31	18 09 17.59 −25 54 38	7.0	−0.11	+0.04	+0.01	+0.01
NGC 6715	18 55 03.3 −30 28 42	18 55 03.50 −30 28 45	4.0	+0.12	−0.04	+0.10	−0.02
NGC 6838	19 53 46.1 +18 46 42	19 53 46.10 +18 46 40	2.0	+0.10	−0.02	−0.06	−0.01
Pal 6	17 43 42.2 −26 13 21	17 43 42.29 −26 13 28	7.1	−0.18	+0.10	−0.12	+0.02
Pal 8	18 41 29.9 −19 49 33	18 41 30.09 −19 49 40	7.5	−0.10	+0.09	−0.18	+0.15
Terzan 1	17 35 47.2 −30 28 54	17 35 47.09 −30 28 56	2.4	−0.18	−0.02	−0.09	+0.01
Terzan 5	17 48 04.9 −24 46 45	17 48 05.00 −24 46 49	4.2	−0.01	−0.02	−0.01	−0.01
Not treated as 2 GCs							
NGC 6426	17 44 54.7 +03 10 13	17 44 54.4 +03 10 12	4.6	...	...	...	...
NGC 6541	18 08 02.2 −43 30 00	18 08 02.20 −43 42 20	740.0	> 3.0	...	...	...
Terzan 12	18 12 15.8 −22 44 31	18 12 15.50 −22 44 27	5.8	...	...	...	...

<sup>a</sup>Colors with center from H96 – those with new center, 50" radius aperture used.

Table 2. Parameters of the King Profile Fits For Galactic GCs<sup>a</sup>

ID	CC <sup>b</sup>	$r_c(V)^c$ (arcsec)	$r_c(J)$ (arcsec)	$\sigma r_c(J)$ (arcsec)	$SB(V)_0^d$ (Mag/sq ")	$A_0(J)$ (DN/sq ")	$\sigma A_0(J)$ (DN/sq ")	$A_0(H)$ (DN/sq ")	$\sigma A_0(H)$ (DN/sq ")	$A_0(K)$ (DN/sq ")	$\sigma A_0(K)$ (DN/sq ")
NGC 362	C?	11.4	11.9	0.8	14.88	1240.9	146.3	1143.1	165.9	991.6	165.5
NGC 1261		23.5	27.0	1.6	17.65	88.8	4.8	86.1	4.8	60.4	3.6
NGC 1851		4.0	8.3	0.8	14.15	1320.9	233.7	1251.0	99.9	922.4	63.7
NGC 1904	C?	9.6	16.6	1.7	16.23	218.2	30.2	219.1	17.0	152.9	11.9
NGC 2298		20.4	27.0	2.2	18.79	41.4	2.0	39.6	1.9	26.5	1.7
NGC 2419		20.9	20.6	1.2	19.83	15.1	0.6	15.9	0.5	10.9	0.4
NGC 2808		15.8	17.4	0.8	15.17	1484.8	103.5	1580.7	85.6	1159.8	49.8
NGC 3201		83.6	97.5	12.8	18.77	44.9	5.4	34.7	7.4	27.1	3.7
NGC 4147		6.0	6.5	0.8	17.63	78.6	12.2	78.9	5.2	52.7	3.8
NGC 4590		41.7	45.1	5.4	18.67	30.1	3.2	35.1	4.9	16.7	1.1
NGC 4833	...	60.0	96.2	14.3	18.45	50.1	4.0	53.3	4.2	36.2	3.4
NGC 5286		17.4	16.8	1.5	16.07	659.8	81.7	711.2	52.9	506.6	40.8
NGC 5634		12.6	11.7	1.0	17.49	102.5	9.7	104.1	6.4	68.5	3.8
NGC 5694		3.7	6.6	0.6	16.34	197.0	27.1	215.2	10.9	144.2	7.3
NGC 5824		3.3	3.9	0.5	15.08	979.3	246.7	1127.9	87.4	691.7	38.2
NGC 5904		23.0	29.5	1.5	16.05	386.3	16.5	343.8	48.0	335.5	41.5
NGC 5927		25.1	33.4	3.6	17.45	200.1	22.0	243.1	26.0	177.3	25.2
NGC 5946	C	4.8	5.4	1.2	17.42	456.1	106.6	537.9	56.6	380.8	52.8
NGC 5986		38.0	36.3	3.6	17.56	161.4	13.6	164.8	12.4	122.1	9.4
NGC 6093		8.9	10.2	0.8	15.19	1038.9	130.9	1107.9	57.3	823.0	40.1
NGC 6121		38.9	112.3	5.4	17.88	111.9	3.8	121.1	4.7	67.5	27.1
NGC 6139		8.1	11.2	1.6	17.30	657.4	139.0	847.2	66.7	636.0	49.0
NGC 6171		32.3	39.4	3.7	18.84	54.1	5.4	65.3	5.6	45.3	4.3
NGC 6205		48.9	46.7	2.5	16.80	214.4	18.0	200.6	13.9	152.9	7.1
NGC 6229		7.9	7.3	0.4	16.99	266.7	23.7	283.1	12.4	198.5	8.4
NGC 6218		44.0	70.6	7.8	18.17	60.8	4.4	57.1	4.9	38.6	4.6
NGC 6235		21.4	19.2	6.1	18.98	52.3	15.7	60.8	8.9	44.7	6.9
NGC 6254		51.3	61.9	5.9	17.69	101.5	8.7	90.9	17.7	57.5	15.0
NGC 6256	C	1.2	22.9	6.6	17.89	85.7	16.2	121.7	18.5	93.6	16.9
NGC 6266	C?	10.8 <sup>e</sup>	25.6	2.9	15.35	1314.3	182.0	1586.9	110.6	1187.8	94.8
NGC 6273		25.7	27.2	1.6	16.82	489.6	37.6	524.6	27.2	366.1	24.4
NGC 6284	C	4.2	7.9	0.7	16.65	383.1	35.5	464.3	31.9	313.9	25.5
NGC 6287		15.8	26.3	2.1	18.33	127.7	7.7	153.6	7.5	116.1	5.7
NGC 6293	C	3.0	11.1	2.0	16.18	393.5	95.8	413.5	43.3	289.2	35.3
NGC 6304		12.6	15.0	1.2	17.34	414.0	41.5	510.5	36.1	363.7	34.4
NGC 6316		10.0	11.7	0.7	17.40	550.0	26.5	733.0	32.0	549.5	29.5
NGC 6325	C	1.8	9.7	1.7	17.56	209.4	42.1	276.4	14.1	219.1	10.5
NGC 6333		34.7	25.0	3.3	17.40	279.0	36.9	312.8	23.9	218.0	19.0
NGC 6341		14.1	16.0	1.0	15.58	581.5	53.1	542.5	52.4	361.6	34.8
NGC 6342	C	3.0	9.3	1.0	17.44	185.9	23.7	227.6	11.9	156.9	15.9
NGC 6352		50.1	34.1	10.3	18.42	56.3	9.5	57.4	6.6	41.3	5.7
NGC 6355	C	3.0	8.7	1.0	18.05	335.1	57.2	440.9	27.1	329.7	22.6
NGC 6356		13.8	17.4	1.0	17.09	354.3	22.1	436.9	18.3	317.4	14.8
NGC 6380	C?	20.4	21.7	2.1	19.96	183.6	14.1	293.3	15.6	237.5	21.1
NGC 6388		7.4	12.7	1.5	14.55	3037.5	614.1	3719.9	205.2	2796.2	161.0
NGC 6402		50.1	47.4	5.1	18.41	144.7	15.0	169.7	11.9	142.0	22.7
NGC 6397	C	3.0	61.5	9.3	15.65	129.6	12.6	121.3	12.8	81.4	8.9
NGC 6401		14.8	11.4	1.1	18.67	248.6	23.3	323.5	30.8	230.2	29.9
NGC 6426		15.8	2.0	1.5	20.37	271.3	361.8	407.5	122.0	297.2	101.8



Table 2—Continued

ID	CC <sup>b</sup>	$r_c(V)^c$ (arcsec)	$r_c(J)$ (arcsec)	$\sigma r_c(J)$ (arcsec)	$SB(V)_0^d$ (Mag/sq ")	$A_0(J)$ (DN/sq ")	$\sigma A_0(J)$ (DN/sq ")	$A_0(H)$ (DN/sq ")	$\sigma A_0(H)$ (DN/sq ")	$A_0(K)$ (DN/sq ")	$\sigma A_0(K)$ (DN/sq ")
NGC 6440		7.6	10.8	1.2	17.02	1792.8	259.4	2818.0	173.4	2332.7	153.9
NGC 6441		6.8	10.6	0.4	14.99	2765.7	138.4	3617.5	100.7	2737.8	72.0
NGC 6453	C	4.2	7.6	1.2	17.35	394.4	55.0	475.6	33.1	336.0	39.6
NGC 6496		63.1	115.9	30.1	20.10	37.2	9.8	37.2	3.8	26.1	2.7
NGC 6517		3.7	8.7	1.9	17.77	547.8	155.9	753.1	88.5	602.7	67.8
NGC 6522	C	3.0	20.2	2.8	16.14	259.3	26.7	315.8	27.0	226.4	21.7
NGC 6535		25.1	11.6	3.1	20.22	23.8	6.5	25.9	3.3	16.5	2.7
NGC 6539		32.3	32.9	3.4	19.31	90.1	9.1	124.8	8.8	110.5	8.7
NGC 6540	...	1.8	1.4	1.6	16.40	1321.0	2909.1	1335.6	269.4	767.2	223.0
NGC 6541	C?	7.2	16.7	1.3	15.58	575.1	48.8	586.4	56.0	411.0	48.3
NGC 6544	C?	13.2	32.0	7.2	17.31	588.0	78.6	694.5	84.5	522.7	63.0
NGC 6553		33.1	32.9	4.4	18.15	614.1	88.1	938.7	139.7	802.6	158.8
NGC 6558	C	1.8	4.2	0.5	17.08	307.6	47.4	325.5	27.6	206.7	28.9
NGC 6569		22.4	19.7	3.7	18.08	244.9	45.0	304.9	41.4	215.2	32.4
NGC 6584		35.5	26.1	3.1	17.79	62.8	8.8	67.5	7.3	40.6	3.8
NGC 6624	C	3.6	7.0	0.7	15.42	1162.1	150.7	1338.5	143.2	1024.5	97.4
NGC 6626		14.5	18.2	1.7	16.08	825.7	98.3	968.4	60.2	687.3	38.1
NGC 6637		20.4	19.2	2.3	16.83	436.6	74.6	525.4	37.0	367.6	30.4
NGC 6638		15.8	12.0	1.0	17.27	309.8	25.8	343.8	28.1	251.8	27.3
NGC 6642	C?	6.0	3.3	1.6	16.68	940.7	799.6	1074.4	134.4	745.2	93.0
NGC 6652		4.3	8.2	1.4	16.31	345.5	72.6	366.1	37.3	245.7	29.0
NGC 6656		85.1	121.8	15.3	17.32	184.7	13.9	172.6	16.3	127.7	11.3
NGC 6681	C	1.8	6.2	1.3	15.28	607.9	189.0	624.3	56.1	420.4	41.3
NGC 6712		56.2	50.7	8.4	18.65	111.7	12.2	128.8	12.6	94.1	9.2
NGC 6715		6.5	7.4	0.3	14.82	1521.6	87.6	1697.2	57.6	1179.3	52.6
NGC 6717	C?	4.8	6.3	0.9	16.48	320.1	68.8	348.2	22.2	239.5	14.9
NGC 6723		56.2	47.6	2.7	17.92	106.3	6.9	108.9	5.0	75.0	3.7
NGC 6749	...	46.2	56.1	4.1	21.54	101.7	3.4	153.4	4.8	124.2	4.3
NGC 6760		20.0	17.3	2.8	18.79	349.9	60.3	517.8	56.0	406.5	56.0
NGC 6779		21.9	33.2	3.4	18.06	88.7	8.2	96.0	7.1	62.7	4.9
NGC 6809		169.7	144.9	10.3	19.13	44.8	2.4	47.3	3.1	30.5	2.0
NGC 6838	...	37.8	48.6	9.0	19.22	60.8	7.6	65.5	7.1	45.8	4.4
NGC 6864		5.8	7.2	0.6	15.55	793.2	109.9	869.3	34.1	619.4	33.7
NGC 6934		14.8	13.7	0.6	17.26	164.3	8.5	162.9	7.0	115.5	3.3
NGC 6981		32.3	26.7	1.2	18.90	32.1	1.3	34.0	2.8	22.8	2.2
NGC 7006		14.5	8.4	0.8	18.50	73.5	8.4	76.9	4.2	52.4	2.2
NGC 7089		20.4	19.7	2.0	15.92	504.2	32.5	522.0	15.0	315.5	33.0
NGC 7099	C	3.6	14.7	1.2	15.28	243.9	25.0	206.9	36.9	131.2	32.1
Pal 2		14.4	12.5	1.0	19.39	14.4	3.3	92.0	3.6	75.0	3.3
Pal 6		39.8	29.8	7.9	21.58	115.6	20.3	195.3	32.3	170.7	32.0
Pal 7		64.6	98.2	15.2	21.66	27.7	2.2	39.9	3.5	22.8	7.0
Pal 8		24.0	26.9	5.9	19.83	19.4	1.6	22.5	1.7	16.5	1.4
Terzan 1	C	2.4	9.8	0.9	25.09	903.7	118.7	1725.4	95.5	1589.4	102.2
Terzan 2	C	1.8	5.7	0.8	21.58	505.5	104.2	922.1	75.1	801.6	68.0
Terzan 5		14.5	6.9	0.5	20.33	3208.7	257.7	7636.8	328.1	8107.6	365.3
Terzan 6	C	3.0	7.8	2.1	20.76	170.4	33.6	386.4	51.7	403.2	65.9
Terzan 9	C	1.8	7.2	1.8	23.21	539.8	148.8	989.5	129.3	869.4	122.1
Terzan 12	...	...	24.0	8.6	...	75.8	8.5	148.4	9.8	132.0	7.8
Djorg 1	...	19.2	8.1	2.3	23.10	64.7	17.1	103.5	13.3	90.8	10.9

Table 2—Continued

ID	CC <sup>b</sup>	$r_c(V)$ <sup>c</sup> (arcsec)	$r_c(J)$ (arcsec)	$\sigma r_c(J)$ (arcsec)	$SB(V)_0$ <sup>d</sup> (Mag/sq ")	$A_0(J)$ (DN/sq ")	$\sigma A_0(J)$ (DN/sq ")	$A_0(H)$ (DN/sq ")	$\sigma A_0(H)$ (DN/sq ")	$A_0(K)$ (DN/sq ")	$\sigma A_0(K)$ (DN/sq ")
HP 1	C	...	15.7	3.7	...	126.1	28.3	178.9	28.4	123.2	21.6
Liller 1	...	...	5.2	0.5	...	858.4	130.1	858.4	130.1	3337.1	220.0
Ton 2	...	32.4	24.8	4.3	22.16	83.9	6.1	132.4	7.9	106.0	8.0
UKS 1	...	9.0	13.5	1.1	25.52	178.9	12.7	547.7	21.1	625.6	25.5

<sup>a</sup>Values are given as measured, without reddening corrections

<sup>b</sup>C denotes known core-collapsed GC, “c?” indicates known probable core-collapsed GC.

<sup>c</sup> $r_c(V)$  preferentially from TKD95, or from H96.  $r_c(V)$  from H96 for all probable core-collapsed GCs.

<sup>d</sup> $SB(V)_0$  from H96.

<sup>e</sup>Beccari *et al.* (2006) gives  $r_c(V) = 19''$  for NGC 6266 and find that it is not a core-collapsed GC.

Table 3. Reddening Corrected Integrated Light IR Colors for Galactic GCs – 50” Radius Aperture

ID	Class <sup>a</sup>	$E(B - V)$ (mag)	[Fe/H] (dex)	[Fe/H] Code <sup>b</sup>	$V - K_s$ (mag)	$J - H$ (mag)	$\sigma(J - H)$ (mag)	$J - K_s$ (mag)	$\sigma(J - K_s)$ (mag)	$J^{50}$ (mag)
NGC 104	BB	0.04	−0.78	KI	2.60	0.55	0.03	0.74	0.03	3.83
NGC 362	FF	0.05	−1.21	KI	2.53	0.52	0.03	0.64	0.03	5.32
NGC 1261	BB	0.10	−1.19	KI	2.05	0.44	0.05	0.50	0.06	7.31
NGC 1851	BB	0.02	−1.12	KI	2.66	0.53	0.03	0.65	0.03	5.90
NGC 1904	BB	0.01	−1.59	KI	2.08	0.49	0.04	0.58	0.05	7.16
NGC 2298	BB	0.14	−2.04	KI	2.39	0.38	0.11	0.52	0.13	8.17
NGC 2419	BB	0.11	−2.12	KI	2.20	0.41	0.32	0.48	0.39	9.48
NGC 2808	BB	0.22	−1.23	ZW,H96	2.50	0.51	0.25	0.62	0.03	4.64
NGC 3201	FF	0.23	−1.40	KI	2.09	0.44	0.05	0.51	0.07	7.02
NGC 4147	BB	0.02	−1.75	KI	1.88	0.41	0.25	0.50	0.31	9.29
NGC 4590	BB	0.05	−2.43	KI	1.94	0.43	0.09	0.45	0.13	8.00
NGC 4833	BB	0.32	−2.04	KI	2.14	0.39	0.04	0.43	0.05	6.46
NGC 5272	BB	0.01	−1.36	CM	2.23	0.52	0.03	0.61	0.04	5.96
NGC 5286	BB	0.24	−1.65	KI	2.26	0.49	0.03	0.55	0.03	5.70
NGC 5634	BB	0.05	−1.88	ZW,H96	1.85	0.36	0.11	0.48	0.13	8.22
NGC 5694	BB	0.09	−2.08	KI	2.26	0.51	0.13	0.56	0.16	8.52
NGC 5824	BB	0.13	−1.85	ZW,H96	2.21	0.46	0.05	0.54	0.06	7.33
NGC 5904	FF	0.03	−1.25	KI	2.19	0.49	0.03	0.61	0.03	5.67
NGC 5927	AF	0.45	−0.37	ZW,H96	3.17	0.58	0.03	0.74	0.03	5.67
NGC 5946	AF	0.54	−1.38	ZW,H96	1.98	0.49	0.04	0.55	0.04	6.67
NGC 5986	BB	0.28	−1.56	KI	2.15	0.47	0.03	0.56	0.03	6.13
NGC 6093	BB	0.18	−1.72	KI	2.23	0.50	0.03	0.59	0.03	5.79
NGC 6121	AA	0.36	−1.15	KI	2.24	0.44	0.03	0.52	0.03	5.77
NGC 6139	AB	0.75	−1.68	ZW,H96	2.49	0.52	0.03	0.55	0.03	5.72
NGC 6171	BB	0.33	−1.02	KI	2.64	0.53	0.04	0.60	0.05	6.86
NGC 6205	BB	0.02	−1.53	KI	2.11	0.46	0.03	0.54	0.03	5.93
NGC 6218	FF	0.19	−1.26	KI	1.92	0.37	0.04	0.46	0.06	6.99
NGC 6229	BB	0.01	−1.43	ZW,H96	2.43	0.53	0.08	0.63	0.10	8.00
NGC 6235	FF	0.36	−1.32	KI	1.95	0.51	0.11	0.57	0.13	8.08
NGC 6254	AA	0.28	−1.43	KI	2.19	0.47	0.03	0.54	0.03	5.91
NGC 6256	AA	1.03	−0.70	H96	3.00	0.61	0.04	0.63	0.05	6.40
NGC 6266	AB	0.47	−1.12	KI	2.33	0.54	0.03	0.62	0.03	4.26
NGC 6273	AB	0.41	−1.79	KI	2.46	0.48	0.03	0.54	0.03	5.11
NGC 6284	BB	0.28	−1.32	ZW,H96	2.47	0.44	0.03	0.52	0.04	6.73
NGC 6287	AB	0.60	−2.05	ZW	2.56	0.53	0.03	0.61	0.03	6.46
NGC 6293	AF	0.41	−1.92	ZW	2.21	0.43	0.03	0.47	0.03	6.20
NGC 6304	AB	0.53	−0.59	ZW	2.69	0.59	0.03	0.71	0.03	5.63
NGC 6316	AB	0.51	−0.55	ZW,H96	3.19	0.65	0.03	0.77	0.03	5.92
NGC 6325	AB	0.89	−1.17	ZW,H96	2.41	0.51	0.05	0.57	0.05	6.71
NGC 6333	BB	0.38	−1.75	ZW,H96	2.17	0.47	0.03	0.53	0.03	5.90
NGC 6341	BB	0.02	−2.38	CMA	2.06	0.45	0.03	0.53	0.03	5.88
NGC 6342	AF	0.46	−0.65	ZW,H96	2.53	0.55	0.05	0.62	0.06	7.14
NGC 6352	FF	0.21	−0.69	KI	1.98	0.48	0.06	0.59	0.07	7.25
NGC 6355	AB	0.75	−1.50	ZW	2.66	0.58	0.03	0.64	0.03	6.36
NGC 6356	BB	0.28	−0.50	ZW,H96	2.65	0.61	0.03	0.70	0.03	6.22
NGC 6380	AA	1.17	−0.50	Z,H96	3.15	0.63	0.03	0.69	0.03	5.51
NGC 6388	BB	0.37	−0.60	ZW,H96	2.65	0.62	0.03	0.75	0.03	4.30
NGC 6397	FF	0.18	−2.11	KI	1.94	0.34	0.03	0.41	0.03	6.05
NGC 6401	AF	0.72	−0.98	ZW,H96	2.89	0.57	0.03	0.64	0.04	6.22
NGC 6402	AF	0.60	−1.39	ZW	2.34	0.48	0.03	0.53	0.03	5.56
NGC 6426	AA	0.36	−2.26	ZW,H96	2.66	0.57	0.27	0.58	0.31	9.17
NGC 6440	AA	1.07	−0.34	ZW,H96	3.06	0.66	0.03	0.74	0.03	4.41
NGC 6441	AB	0.47	−0.53	ZW,H96	2.68	0.62	0.03	0.74	0.03	4.47
NGC 6453	AF	0.66	−1.53	ZW	2.61	0.49	0.03	0.58	0.03	6.23
NGC 6496	FF	0.15	−0.69	KI	3.03	0.48	0.12	0.56	0.14	8.24
NGC 6517	AA	1.08	−1.37	ZW,H96	3.22	0.48	0.03	0.49	0.03	6.02
NGC 6522	AB	0.48	−1.36	KI	2.50	0.57	0.04	0.65	0.04	5.84
NGC 6528	AB	0.54	0.07	Car	4.04	0.65	0.03	0.78	0.03	5.50
NGC 6535	FF	0.34	−1.76	KI	2.11	0.45	0.22	0.43	0.28	8.90
NGC 6539	AB	0.97	−0.66	ZW	2.79	0.52	0.04	0.64	0.04	6.17
NGC 6540	AA	0.60	−1.20	H96	3.95	0.50	0.04	0.55	0.04	6.63
NGC 6541	FF	0.14	−1.78	KI	2.33	0.41	0.13	0.42	0.15	5.66
NGC 6544	AF	0.73	−1.35	KI	2.40	0.49	0.03	0.59	0.03	5.34
NGC 6553	AF	0.63	−0.06	CohCar	3.73	0.69	0.03	0.87	0.03	4.53
NGC 6558	AF	0.44	−1.44	ZW	2.35	0.49	0.06	0.54	0.07	7.29

Table 3—Continued

ID	Class <sup>a</sup>	$E(B - V)$ (mag)	[Fe/H] (dex)	[Fe/H] Code <sup>b</sup>	$V - K_s$ (mag)	$J - H$ (mag)	$\sigma(J - H)$ (mag)	$J - K_s$ (mag)	$\sigma(J - K_s)$ (mag)	$J^{50}$ (mag)
NGC 6569	AF	0.55	−0.86	ZW	2.57	0.59	0.03	0.65	0.03	6.03
NGC 6584	BB	0.10	−1.49	ZW,H96	2.33	0.45	0.08	0.51	0.09	7.78
NGC 6624	BB	0.28	−0.69	KI	2.82	0.60	0.03	0.73	0.03	5.85
NGC 6626	AB	0.40	−1.12	KI	2.43	0.52	0.03	0.60	0.03	5.02
NGC 6637	BB	0.16	−0.80	KI	2.99	0.61	0.03	0.75	0.03	5.85
NGC 6638	AF	0.40	−0.92	KI	2.36	0.53	0.03	0.61	0.03	6.44
NGC 6642	AF	0.41	−1.35	ZW,H96	2.67	0.60	0.03	0.65	0.04	6.79
NGC 6652	FF	0.09	−0.69	ZW,H96	2.51	0.52	0.05	0.60	0.06	7.37
NGC 6656	BB	0.32	−1.64	ZW,H96	2.37	0.41	0.03	0.50	0.03	5.03
NGC 6681	BB	0.07	−1.54	KI	2.04	0.45	0.04	0.53	0.05	7.09
NGC 6712	AB	0.45	−1.02	KI	2.26	0.44	0.03	0.50	0.04	6.43
NGC 6715	BB	0.15	−1.41	KI	2.40	0.55	0.03	0.66	0.03	5.92
NGC 6717	BB	0.22	−1.21	KI	2.60	0.39	0.05	0.49	0.06	7.33
NGC 6723	BB	0.05	−1.03	KI	2.42	0.49	0.03	0.57	0.04	6.74
NGC 6749	AA	1.50	−1.60	H96	2.86	0.48	0.04	0.44	0.03	5.62
NGC 6760	AF	0.77	−0.52	ZW	3.06	0.63	0.03	0.72	0.03	5.59
NGC 6779	BB	0.20	−1.94	ZW	2.11	0.47	0.04	0.53	0.05	7.11
NGC 6809	BB	0.08	−1.82	KI	2.43	0.38	0.07	0.44	0.09	7.62
NGC 6838	FF	0.25	−0.73	KI	2.72	0.47	0.06	0.53	0.07	7.32
NGC 6864	BB	0.16	−1.16	ZW,H96	2.36	0.52	0.03	0.61	0.03	6.73
NGC 6934	BB	0.10	−1.54	ZW	2.03	0.46	0.06	0.55	0.07	7.50
NGC 6981	FF	0.05	−1.36	KI	1.94	0.44	0.14	0.53	0.17	8.51
NGC 7006	BB	0.05	−1.63	ZW,H96	2.34	0.33	0.23	0.53	0.26	9.09
NGC 7089	FF	0.06	−1.51	KI	1.63	0.47	0.03	0.57	0.03	6.18
NGC 7099	AA	0.03	−2.32	KI	2.09	0.41	0.03	0.49	0.04	6.84
IC 1276	AA	1.08	−0.73	H96	3.09	0.62	0.08	0.67	0.09	6.54
Pal 2	AA	1.24	−1.30	H96	...	0.56	0.13	0.56	0.14	7.65
Pal 6	AA	1.46	−1.09	Z,H96	3.51	0.67	0.09	0.72	0.10	5.31
Pal 8	FF	0.32	−0.48	ZW	3.00	0.54	0.13	0.62	0.14	7.86
Terzan 1	AA	2.28	−1.30	AZ,H96	...	0.52	0.03	0.44	0.03	3.88
Terzan 2	AA	1.57	−0.40	AZ,H96	...	0.58	0.03	0.63	0.03	5.54
Terzan 5	AA	2.15	0.00	AZ,H96	3.63	0.75	0.03	0.80	0.03	3.26
Terzan 6	AA	2.14	−0.50	AZ,H96	...	0.74	0.06	0.77	0.05	5.39
Terzan 9	AA	1.87	−2.00	AZ,H96	...	0.57	0.03	0.55	0.03	4.96
Terzan12	AA	2.06	−0.50	H96	...	0.73	0.06	0.72	0.06	5.52
HP 1	AF	0.74	−1.55	AZ,H96	...	0.74	0.09	0.85	0.10	6.09
UKS 1	AA	3.09	−0.50	ZW,H96	...	0.68	0.03	0.61	0.03	4.25
Djorg 1	AA	1.44	−2.00	H96	4.72 <sup>c</sup>	0.65	0.13	0.77	0.12	6.37
Ton 2	AA	1.24	−0.50	H96	4.17 <sup>c</sup>	0.62	0.05	0.66	0.05	5.95
Liller 1	AA	3.06	0.22	AZ,H96	...	0.77	0.03	0.78	0.03	4.18

<sup>a</sup>Class( $V - K_s$ ), Class(IR), B = Best, F = Fair and not Best, A = All, i.e. not B or F

<sup>b</sup>[Fe/H] sources: KI = Kraft & Ivans (2003), AZ = Armandroff & Zinn (1988), Z = Zinn (1985), H96 = Harris (1996) and references therein, Coh = Cohen *et al.* (1999), Car = Carretta *et al.* (2001), CM = Cohen & Melendez (2005), CMa = Cohen & Melendez, in preparation.

<sup>c</sup>These GCs appear to have problems in the  $V$  SB zero point or substantial errors in  $E(B - V)$ .

Table 4. Numbers of Galactic GCs in Our Samples

Group	$E(B - V)$ (Below) (mag)	SNR( $K_s$ )(min) <sup>a</sup>	Number
$J - K_s$			
Best	1.0	10	52
Fair	1.0	5	82
All	...	...	105 <sup>b</sup>
$V - K_s$			
Best	0.40	10	38
Fair	0.40	5	53
All	...	...	96 <sup>bc</sup>

<sup>a</sup>SNR determined from fit King profile surface brightness evaluated in central 5" of GC. Actual SNR from pseudo-aperture photometry is much higher.

<sup>b</sup>This includes 47 Tuc, with IR data from the 2MASS Large Galaxy Atlas.

<sup>c</sup>Nine of the sample GCs have no accurate  $V$  surface brightness profile.

Table 5. Aaronson, Malkan & Kleinmann 1978 Integrated Light Photometry of Galactic GCs

ID	$V - K^a$ (mag – Obs.)	$J - H^a$ (mag – Obs)	$H - K_s^a$ (mag – Obs)	CO Index <sup>a</sup> (mag – Dered.)	$H_2O$ Index <sup>a</sup> (mag – Dered.)
Low Red Calibs					
NGC 5024	2.19	0.52	0.11	0.016	0.063
NGC 5272	2.22	0.55	0.08	0.021	0.024
NGC 5904	2.33	0.60	0.10	0.044	0.013
NGC 6205	2.62	0.59	0.10	0.031	0.034
NGC 6254	3.10 <sup>b</sup>	0.65	0.13	0.022	0.044
NGC 6341	2.20	0.48	0.10	−0.006	0.022
NGC 6838	3.70 <sup>b</sup>	0.72	0.17	0.075	0.045
NGC 7006	2.37	0.53	0.09	...	...
NGC 7078	2.16	0.47	0.11	−0.006	0.017
NGC 7089	2.38	0.53	0.09	0.024	0.031
NGC 7099	2.09	0.49	0.09	0.007	0.039
High Red Calibs					
NGC 6121	3.54	0.75	0.17	0.065	0.015
NGC 6171	4.03 <sup>b</sup>	0.78	0.19	0.089	0.052
NGC 6656	3.16	0.69	0.14	0.038	0.040
Low Red					
NGC 1904	2.24 <sup>c</sup>	0.52	0.07	...	...
NGC 2419	2.17	0.54	0.04	...	...
NGC 5634	2.44 <sup>c</sup>	0.53	0.11	0.054	0.051
NGC 6093	2.92	0.61	0.11	0.011	0.042
NGC 6218	2.68	0.62	0.11	0.041	0.092
NGC 6229	2.50	0.58	0.08	...	...
NGC 6356	3.65	0.76	0.19	0.063	0.048
NGC 6637	3.23	0.80	0.17	0.073	0.064
NGC 6715	2.78	0.62	0.14	...	...
NGC 6864	2.93	0.62	0.12	...	...
NGC 6934	2.51	0.56	0.10	0.001	0.028
NGC 6981	2.72 <sup>b</sup>	0.63	0.10	...	...

Table 5—Continued

ID	$V - K^a$ (mag – Obs.)	$J - H^a$ (mag – Obs)	$H - K_s^a$ (mag – Obs)	CO Index <sup>a</sup> (mag – Dered.)	$H_2O$ Index <sup>a</sup> (mag – Dered.)
High Red					
NGC 6273	3.37	0.66	0.15	0.019	0.023
NGC 6284	3.05	0.70	0.13	...	...
NGC 6293	3.11	0.62	0.11	...	...
NGC 6333	3.27	0.76	0.19	0.036	0.052
NGC 6402	3.89	0.76	0.19	0.045	0.064
NGC 6440	5.68	1.04	0.31	0.100	0.055
NGC 6544	4.50	0.84	0.21	0.038	0.015
NGC 6626	3.34	0.72	0.19	0.057	0.055
NGC 6638	3.83	0.77	0.15	...	...
NGC 6712	3.50	0.72	0.17	0.092	0.064
NGC 6779	2.92	0.58	0.13	0.033	0.036
Others <sup>d</sup>					
NGC 288	2.11	0.60	0.13	...	...
NGC 1851	2.51	0.63	0.10	...	...
NGC 2298	...	0.59	0.13	...	...
NGC 2808	2.96	0.69	0.16	...	...
NGC 4147	...	0.47	0.12	...	...
NGC 5286	2.98	0.63	0.16	...	...
NGC 5694	2.39	0.53	0.08	...	...
NGC 5824	2.53	0.59	0.12	...	...
NGC 5927	...	0.89	0.28	...	...
NGC 5986	2.93	0.66	0.17	...	...
NGC 6139	4.42	0.80	0.24	...	...
NGC 6304	4.63	0.92	0.26	...	...
NGC 6316	4.80	0.82	0.22	...	...
NGC 6342	4.05	0.81	0.22	...	...
NGC 6355	4.49	0.85	0.25	...	...
NGC 6388	3.69	0.78	0.21	...	...

Table 5—Continued

ID	$V - K^a$ (mag – Obs.)	$J - H^a$ (mag – Obs)	$H - K_s^a$ (mag – Obs)	CO Index <sup>a</sup> (mag – Dered.)	$H_2O$ Index <sup>a</sup> (mag – Dered.)
NGC 6441	3.90	0.83	0.22	...	...
NGC 6517	5.17	0.86	0.26	...	...
NGC 6522	3.48	0.74	0.17	...	...
NGC 6528	4.52	0.89	0.23	...	...
NGC 6535	3.36	0.89	0.11	...	...
NGC 6539	5.45	1.00	0.28	...	...
NGC 6553	5.51	1.04	0.32	...	...
NGC 6624	3.61	0.78	0.21	...	...
NGC 6642	3.40	0.74	0.16	...	...
NGC 6681	2.52	0.61	0.12	...	...
NGC 6749	6.97	1.03	0.46	...	...
NGC 6760	4.98	0.95	0.28	...	...

<sup>a</sup>Observed colors of Aaronson, Malkan & Kleinmann, about 1977, unpublished, see brief description in Aaronson, Cohen, Mould & Malkan (1978). These are in the CIT system, not the 2MASS system. Part of this dataset, in the form of reddening corrected broad band colors, was published by Brodie & Huchra (1990).

<sup>b</sup>Discrepancy in  $V - K$  between the two independent archives of the 1977 data exceeds 0.2 mag. See text for details.

<sup>c</sup> $V - K$  not used by Aaronson, Cohen, Mould & Malkan (1978).

<sup>d</sup>None of these were used by Aaronson, Cohen, Mould & Malkan (1978).



Table 6. Comparison of IR Integrated Light Photometry of Galactic GCs

Group	Number in Common	Mean $\Delta$ (mag) 2MASS(2006) – AMK(1978) <sup>a</sup>	$\sigma$ [[Mean $\Delta$ ]] (mag)
<hr/>			
$V - K_s$			
Calibrators	12	−0.15	0.25
All	35	−0.07	0.26
$E(B - V) < 0.40$ mag	27	−0.12	0.25
<hr/>			
$J - K_s$			
Calibrators	12	−0.14	0.08
All	35	−0.13	0.07
$E(B - V) < 1.0$ mag	34	−0.13	0.07

<sup>a</sup>Aaronson, Malkan & Kleinmann (1978), unpublished, see brief description in Aaronson, Cohen, Mould & Malkan (1978).

Table 7. Comparison of IR Integrated Light Photometry of Galactic GCs From 2MASS – Us vs. Nantais *et al.* (2006)

Group	Number in Common	Mean $\Delta$ (mag) 2MASS(us) – Nantais <i>et al.</i> (2006)	$\sigma$ [[Mean $\Delta$ ]] (mag)
<hr/>			
$V - K_s$			
All “reliable” <sup>a</sup>	58	+0.63	0.52
<hr/>			
$J - K_s$			
All “reliable” <sup>a</sup>	59	−0.01	0.12
<hr/>			
$J - H_s$			
All “reliable” <sup>a</sup>	59	−0.02	0.13

<sup>a</sup>Includes only those GCs regarded as “reliable” by Nantais *et al.* (2006). Those with  $V - J < 0$ , among others, are excluded.



Table 8—Continued

Group	Number GCs	Order of Fit <sup>a</sup>	$A(0)$ (mag)	$A(1)$	$A(2)$ (mag <sup>-1</sup> )	$\sigma$ About Fit (mag)
Best	52	1	0.638	0.094	...	0.05
Best	52	2	0.673	0.167	0.030	0.05
Fair	82	1	0.646	0.104	...	0.06
Fair	82	2	0.669	0.155	0.022	0.06
Fair + High [Fe/H] <sup>b</sup>	84	2	0.672	0.159	0.023	0.06

<sup>a</sup>Fit is linear (1) or quadratic (2)

<sup>b</sup>Adds those GCs in our sample with [Fe/H] > -0.2 dex that are not already included. See text for details.

<sup>c</sup> $\sigma$  rises to  $\sim 0.30$  mag if a linear fit is used.

<sup>d</sup>1977 fit transformed from Johnson to 2MASS colors.

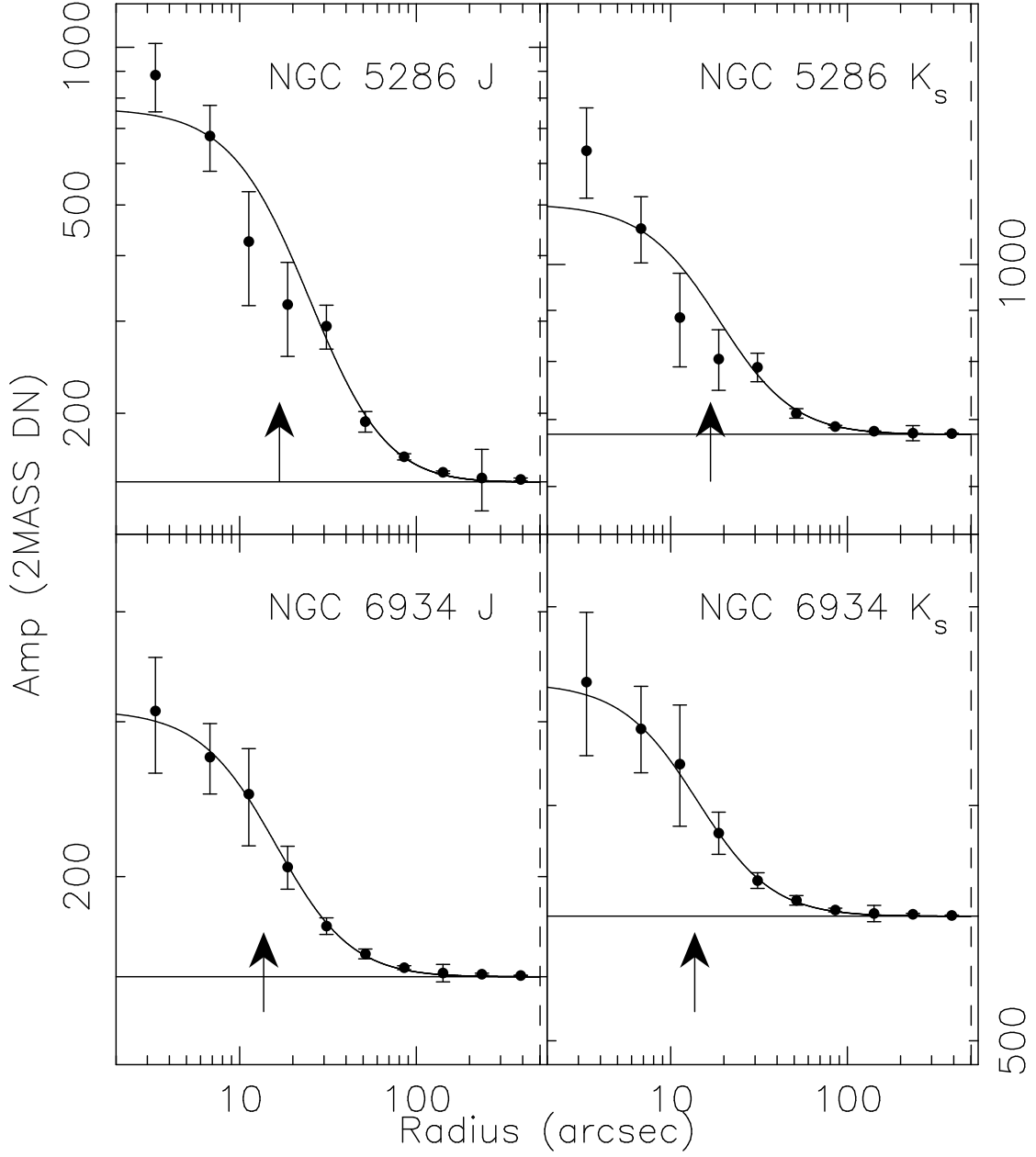


Fig. 1.— The surface brightness for the 30th brightest (top) and 30th faintest (bottom) GCs in our sample are shown for  $J$  (left panels) and for  $K_s$  (right panels). The fit King profiles are also shown. An arrow marks  $r_c(J)$  and a vertical dashed line indicates the tidal radius. The horizontal line indicates the background.

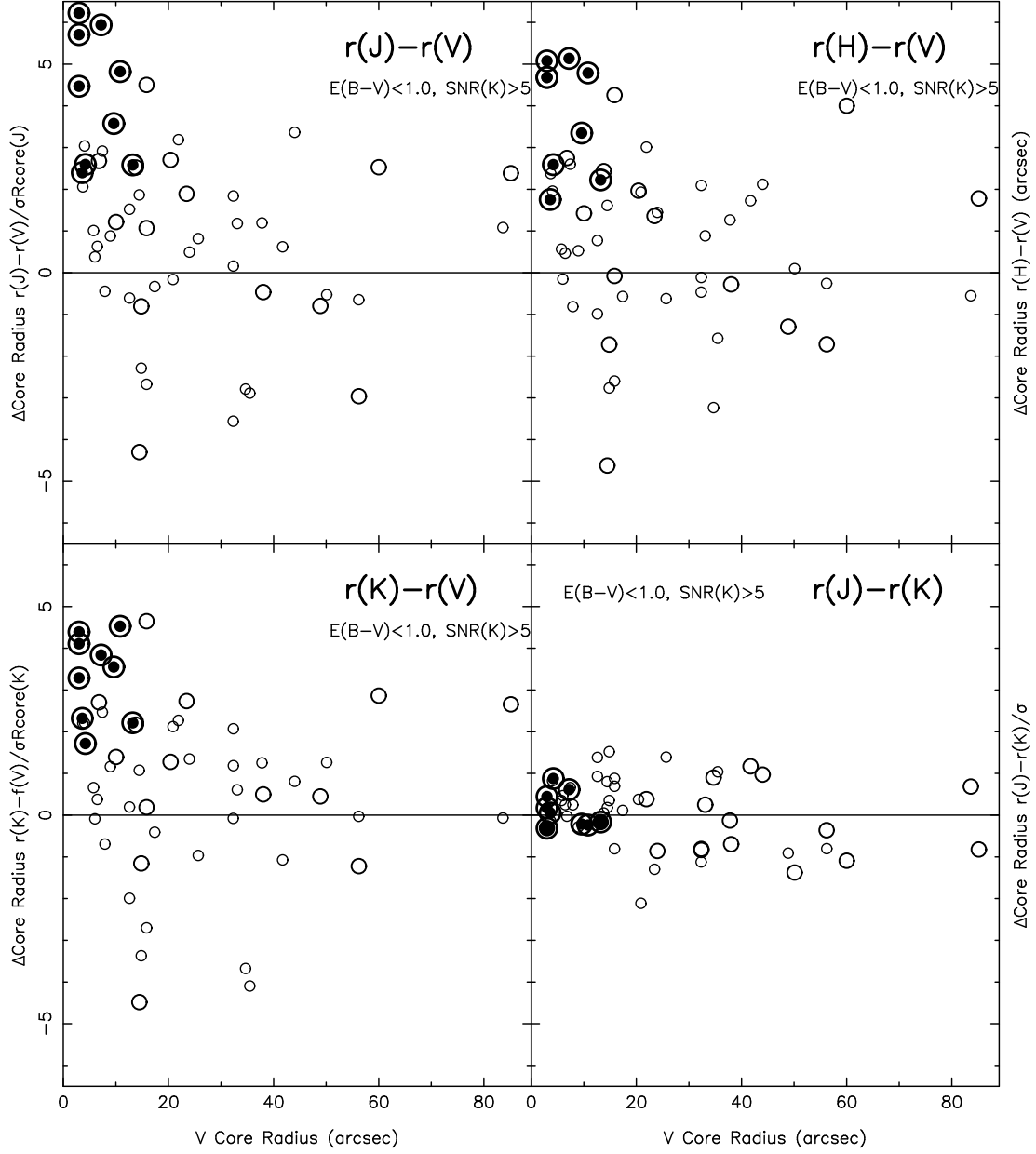


Fig. 2.— The difference in core radius between  $J$ ,  $H$  or  $K_s$  and  $V$  divided by the uncertainty of this difference is shown as a function of the  $V$  core radius. The lower right panel shows the case of  $r_c(J)$  as compared to  $r_c(K_s)$ . A minimum uncertainty in each core radius of  $1.0''$  is assumed. Probable core collapsed GCs are circled; their  $r_c(V)$  are from H96; all others are from TKD95.

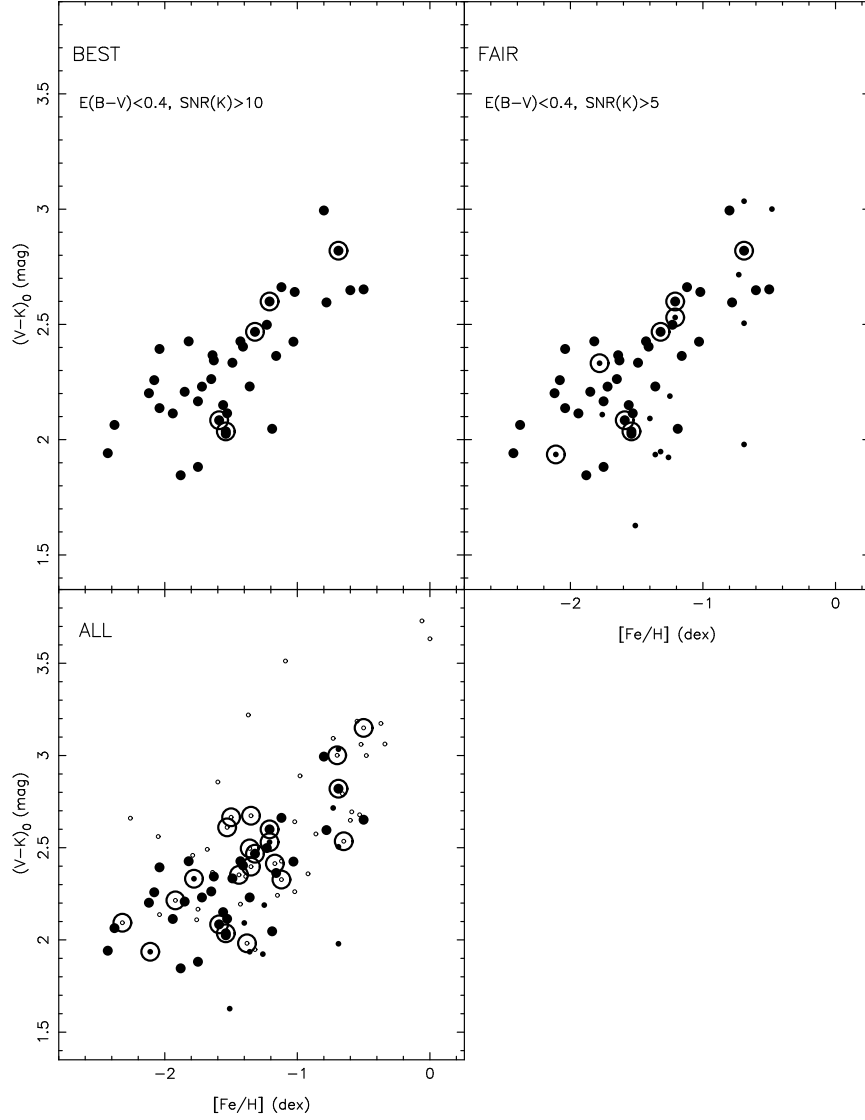


Fig. 3.— Dereddened  $V - K_s$  colors are shown as a function of  $[\text{Fe}/\text{H}]$  for the sample of “best” (large filled circles), “fair” (the “best” sample plus smaller filled circles) and “all” (adding in GCs denoted by small open circles) GCs with IR surface brightness profiles from 2MASS derived here. Clusters which are, or may be, core collapsed (as indicated in TKD95) are circled. An aperture  $50''$  in radius is used.

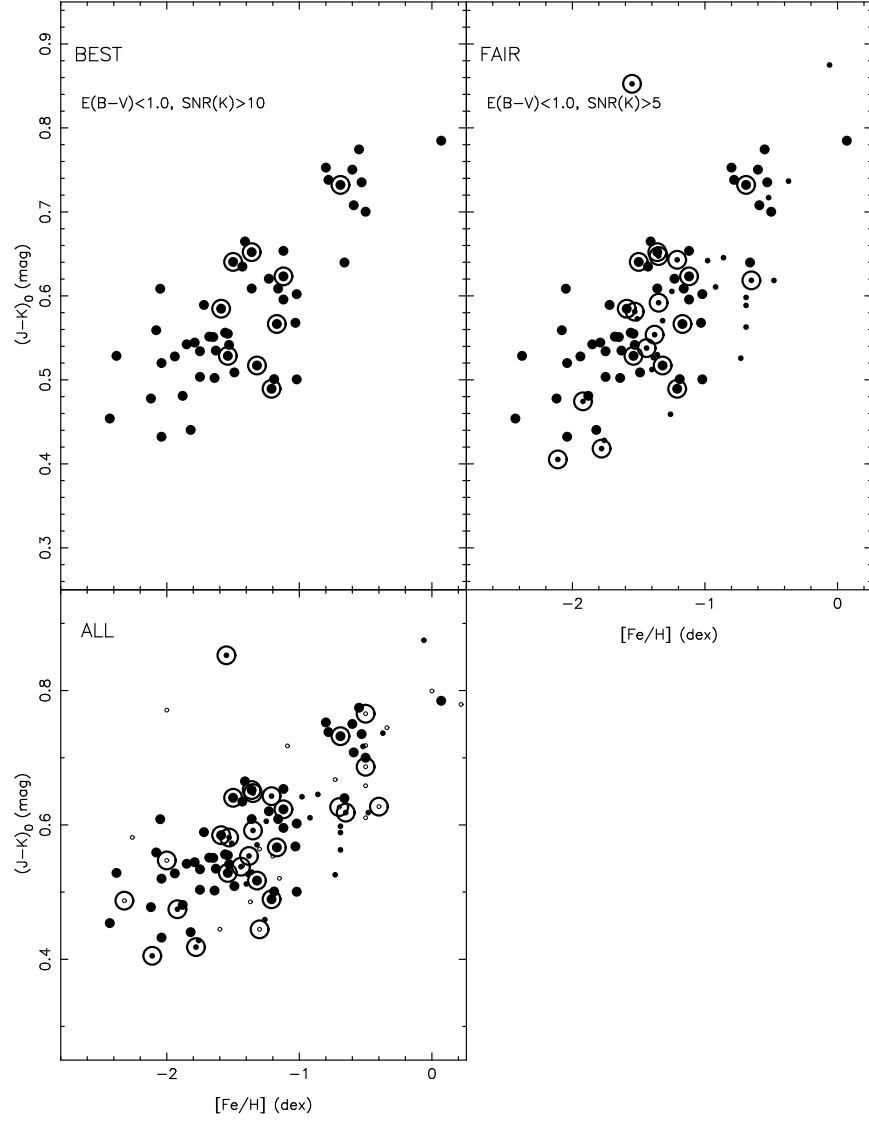


Fig. 4.— Dereddened  $J - K_s$  colors are shown as a function of  $[\text{Fe}/\text{H}]$  for the sample of “best”, “fair” and “all” GCs with IR surface brightness profiles from 2MASS derived here. The symbols are those of Fig. 3. An aperture  $50''$  in radius is used. The red outlier appearing in the “fair” sample is HP 1.

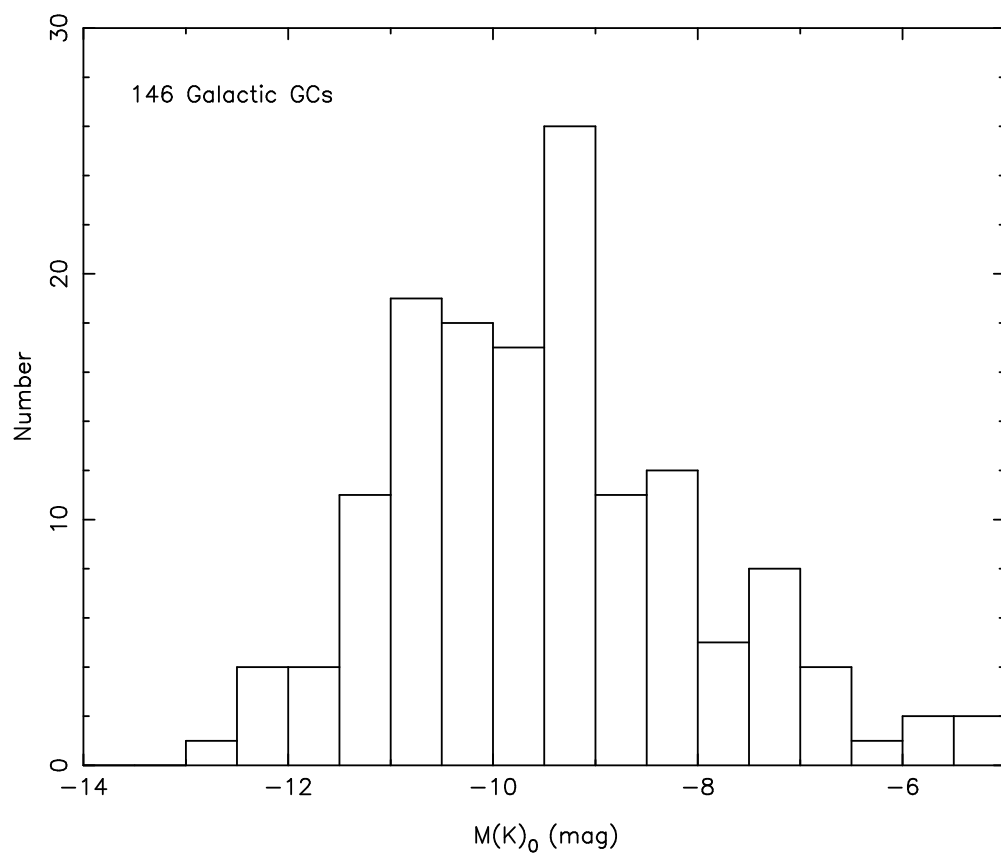


Fig. 5.— The luminosity function at  $K_s$  is shown for 146 of the Galactic globular clusters.



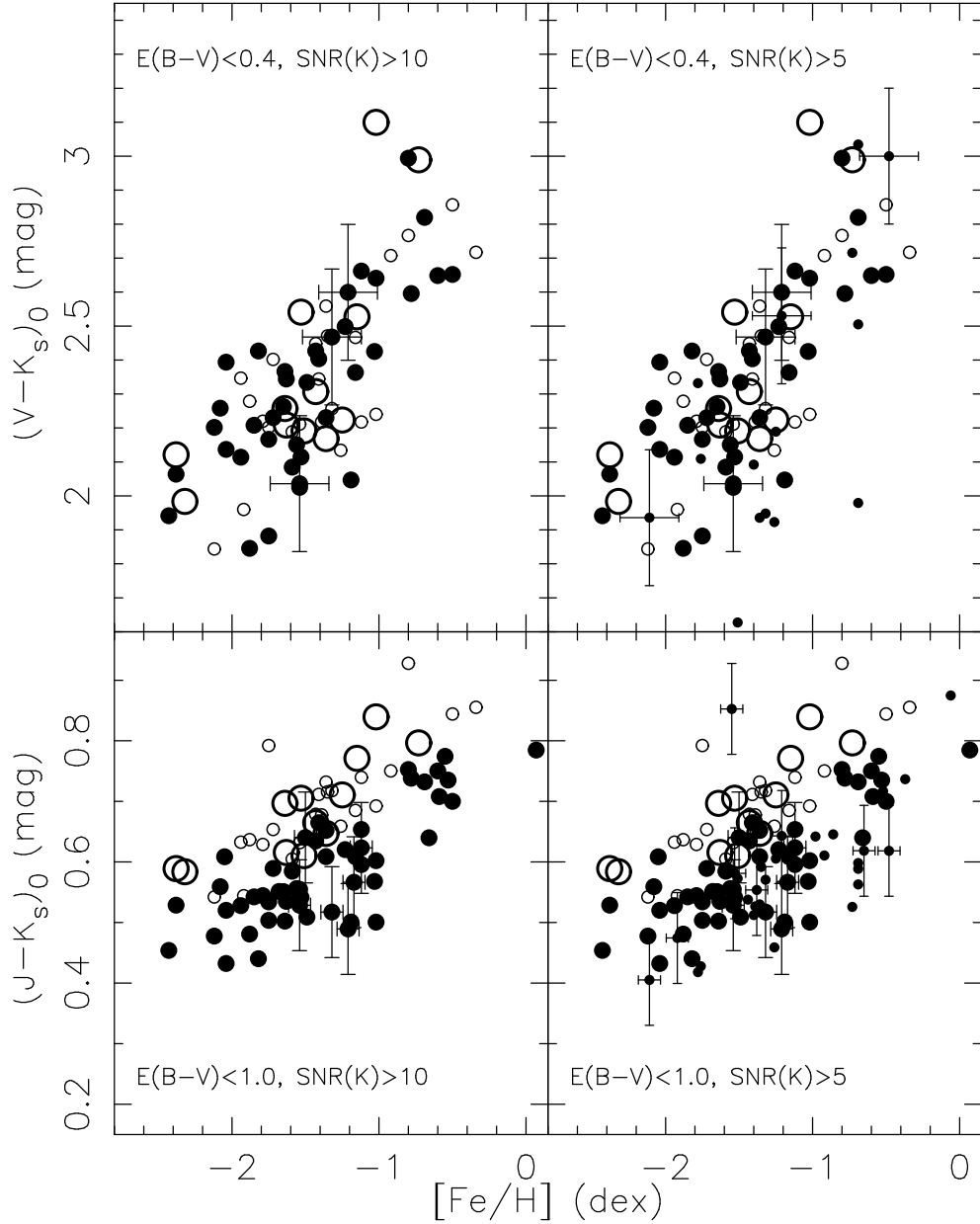


Fig. 6.— The top panels show  $(V - K_s)_0$  versus  $[\text{Fe}/\text{H}]$  from our “best” (left, large filled circles) and “fair” (right, small filled circles) samples; the bottom panels show the same for  $(J - K_s)_0$ . A  $50''$  radius circular aperture is used. Core collapsed GCs are marked with crosses. The 1978 data of Aaronson, Malkan & Kleinmann, transformed as described in §6.1, is superposed (large open circles are their calibrating clusters which they believed to have accurate metallicities and reddenings; smaller open circles are other GCs used in Aaronson, Cohen, Mould & Malkan (1978).

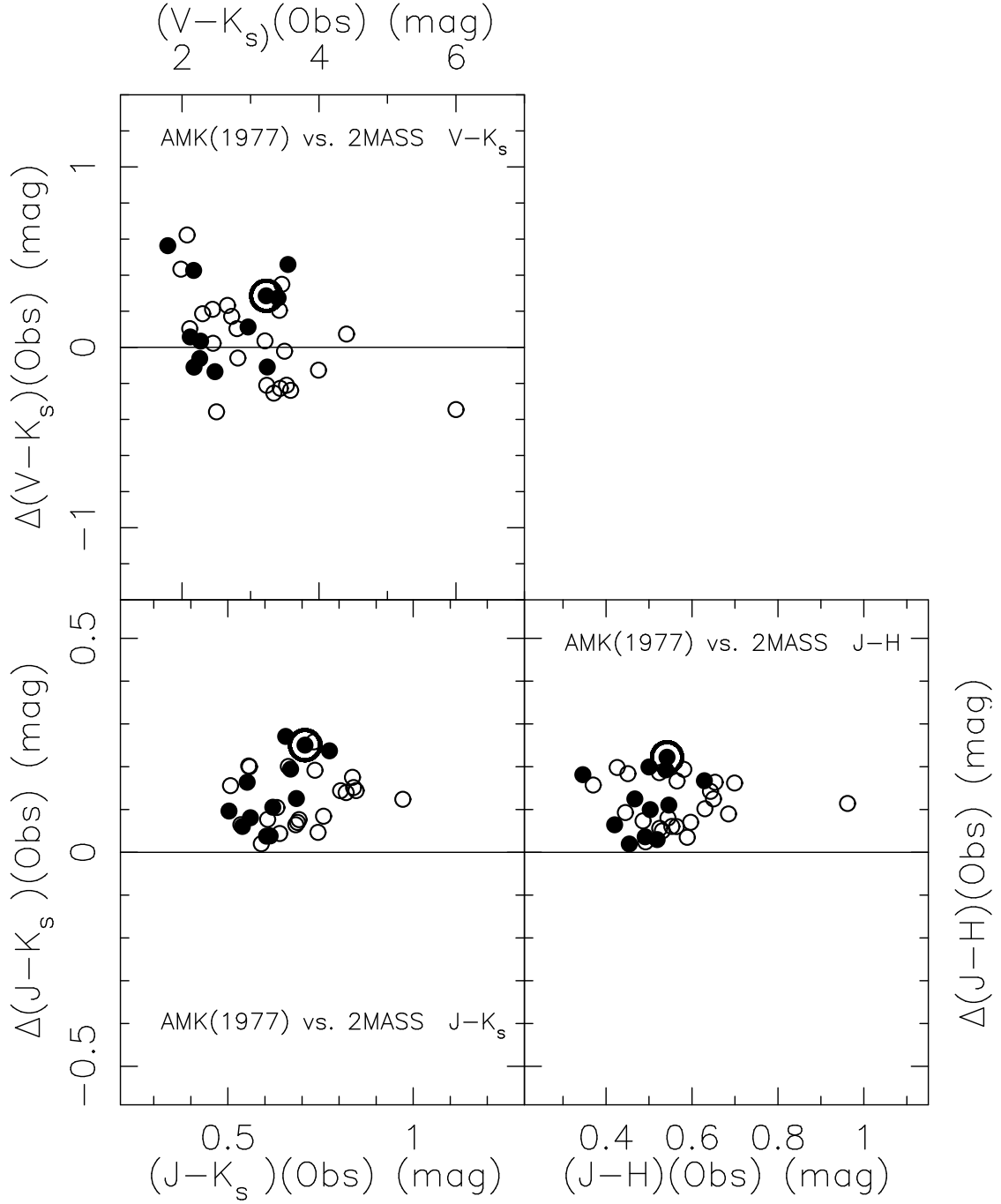


Fig. 7.— The difference between the 1978 colors of Aaronson, Malkan & Kleinmann and the 2MASS colors presented here, as observed and in the 2MASS system for both, are shown for  $V-K_s$ ,  $J-K_s$  and  $J-H$  as a function of our 2MASS colors.

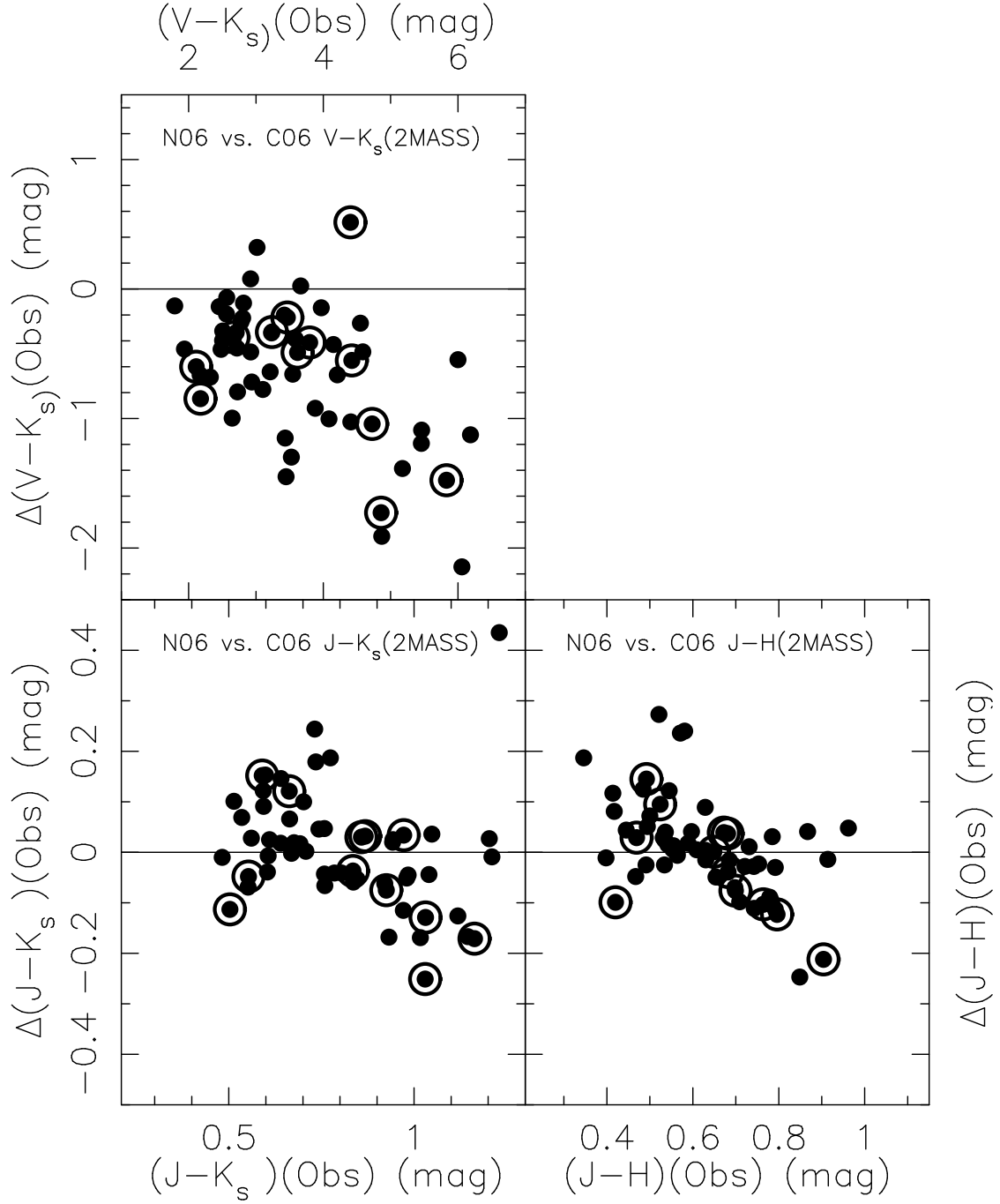


Fig. 8.— The difference between the colors of Nantais *et al.* (2006) and those presented here, as observed and in the 2MASS system for both, are shown for  $V - K_s$  (upper panels) and for  $J - K_s$  (lower panels) as a function of our observed 2MASS colors. Core collapse GCs are circled.

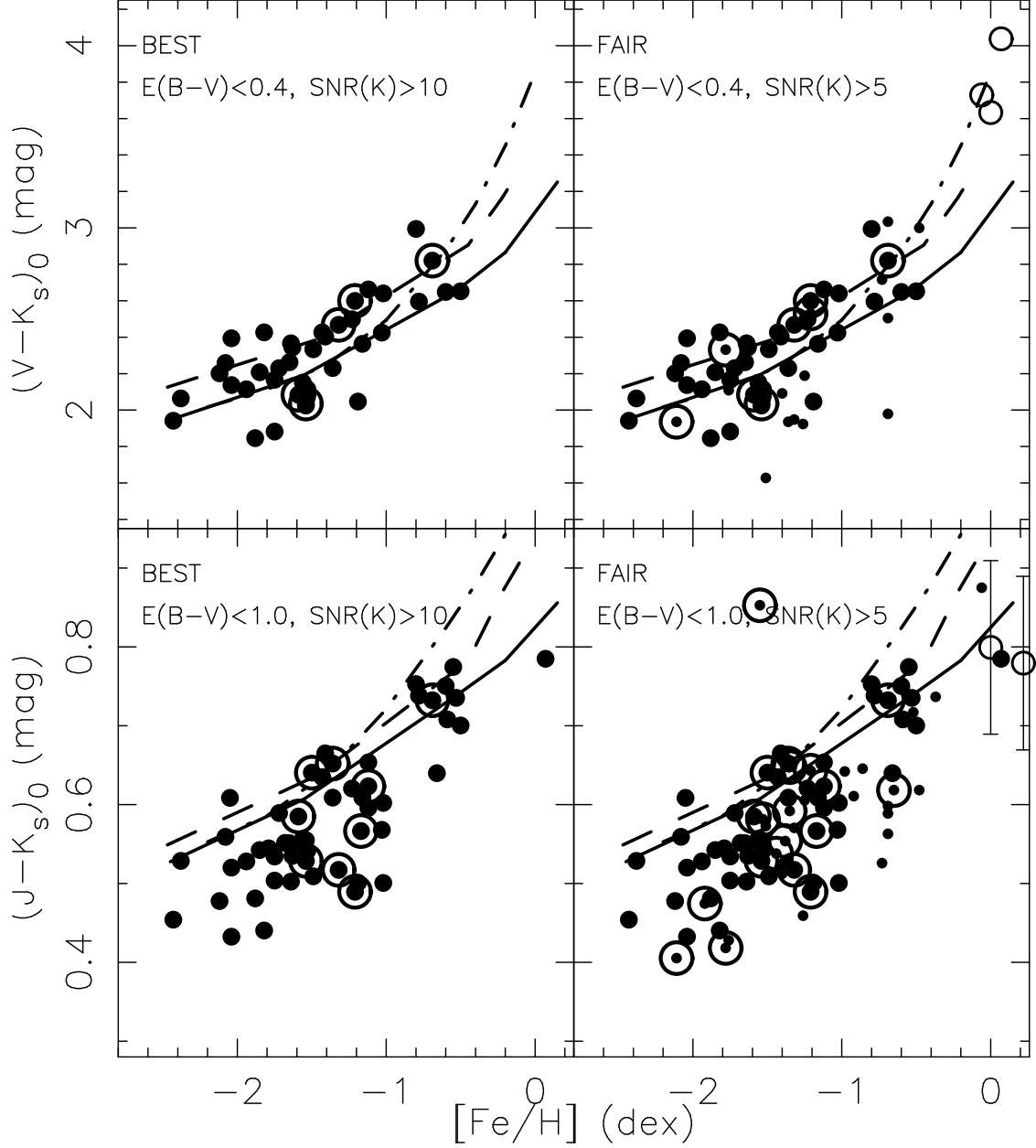


Fig. 9.— Our derived dereddened 2MASS integrated light colors  $(V - K_s)_0$  and  $(J - K_s)_0$  are shown as a function of  $[\text{Fe}/\text{H}]$  for the “best” and “fair” Galactic GC samples. Predicted SSP colors of a 11 Gyr model from Maraston (2005) (solid curve) and a 15 Gyr model from Worthey (1994) (dot-dashed curve), as well as a 12.5 Gyr model of Buzzoni (1989) (long dashed curve) are superposed. These have been transformed from the Johnson into the 2MASS system and  $[\text{Fe}/\text{H}]$  values for each of the model curves have been adjusted for the  $\alpha$ -element enhancement characteristic of Galactic GCs. Additional GCs with  $[\text{Fe}/\text{H}] > -0.2$  dex which do not meet the criteria for the “fair” sample are shown in the right panels as open circles. Error bars are shown for the two of these which are heavily reddened in the lower right panel, see text for details.